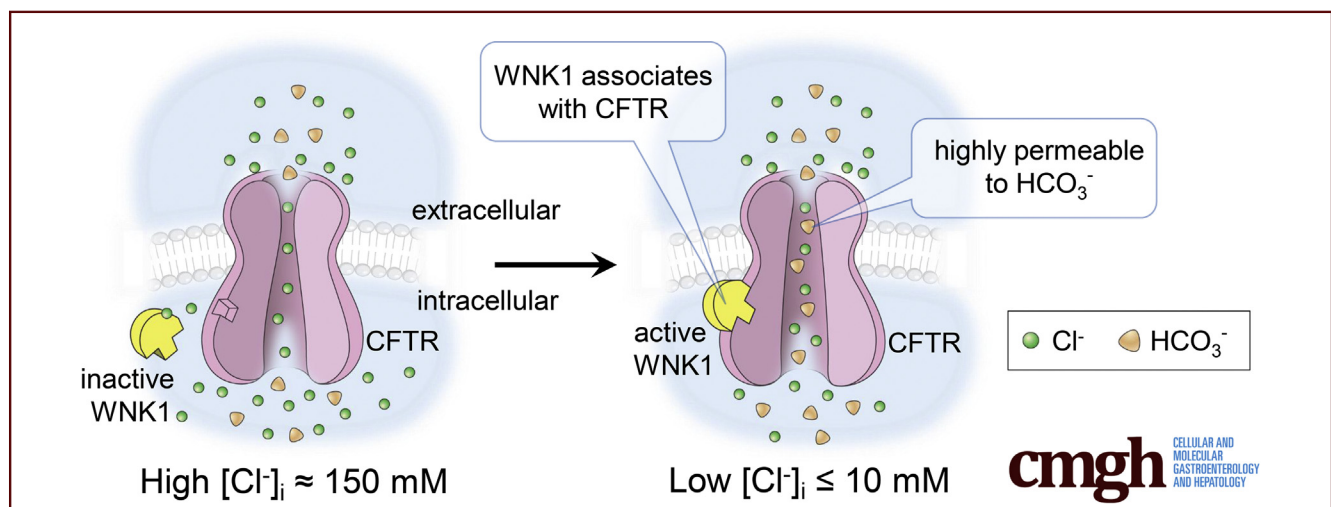


ORIGINAL RESEARCH

Regulation of CFTR Bicarbonate Channel Activity by WNK1:
Implications for Pancreatitis and CFTR-Related Disorders

Yonjung Kim,^{1,*} Ikhyun Jun,^{1,2,*} Dong Hoon Shin,¹ Jihoon G. Yoon,¹ He Piao,¹ Jinsei Jung,^{1,3} Hyun Woo Park,⁴ Mary Hongying Cheng,⁵ Ivet Bahar,⁵ David C. Whitcomb,⁶ and Min Goo Lee¹

¹Department of Pharmacology, Brain Korea 21 PLUS Project for Medical Sciences, Severance Biomedical Science Institute, Yonsei University College of Medicine, Seoul, Korea; ²Institute of Vision Research, Department of Ophthalmology, Yonsei University College of Medicine, Seoul, Korea; ³Department of Otorhinolaryngology, Yonsei University College of Medicine, Seoul, Korea; ⁴Department of Biochemistry, College of Life Science and Biotechnology, Yonsei University, Seoul, Korea; ⁵Department of Computational & Systems Biology, University of Pittsburgh, Pittsburgh, Pennsylvania; and ⁶Division of Gastroenterology, Hepatology and Nutrition, Department of Medicine, University of Pittsburgh, Pittsburgh, Pennsylvania



SUMMARY

This study demonstrates that the N-terminal region of with-no-lysine kinase 1 increases the bicarbonate permeability and conductance of cystic fibrosis transmembrane conductance regulator anion channels via an intracellular chloride concentration-dependent physical association, which facilitates transepithelial bicarbonate secretion. Defects in this process underlie the pathogenesis of some cystic fibrosis transmembrane conductance regulator-related disorders.

BACKGROUND & AIMS: Aberrant epithelial bicarbonate (HCO_3^-) secretion caused by mutations in the cystic fibrosis transmembrane conductance regulator (CFTR) gene is associated with several diseases including cystic fibrosis and pancreatitis. Dynamically regulated ion channel activity and anion selectivity of CFTR by kinases sensitive to intracellular chloride concentration ($[\text{Cl}^-]_i$) play an important role in epithelial HCO_3^- secretion. However, the molecular mechanisms of how $[\text{Cl}^-]_i$ -dependent mechanisms regulate CFTR are unknown.

METHODS: We examined the mechanisms of the CFTR HCO_3^- channel regulation by $[\text{Cl}^-]_i$ -sensitive kinases using an integrated electrophysiological, molecular, and computational approach

including whole-cell, outside-out, and inside-out patch clamp recordings and molecular dissection of WNK1 and CFTR proteins. In addition, we analyzed the effects of pancreatitis-causing CFTR mutations on the WNK1-mediated regulation of CFTR.

RESULTS: Among the WNK1, SPAK, and OSR1 kinases that constitute a $[\text{Cl}^-]_i$ -sensitive kinase cascade, the expression of WNK1 alone was sufficient to increase the CFTR bicarbonate permeability ($P_{\text{HCO}_3^-}/P_{\text{Cl}^-}$) and conductance ($G_{\text{HCO}_3^-}$) in patch clamp recordings. Molecular dissection of the WNK1 domains revealed that the WNK1 kinase domain is responsible for CFTR $P_{\text{HCO}_3^-}/P_{\text{Cl}^-}$ regulation by direct association with CFTR, while the surrounding N-terminal regions mediate the $[\text{Cl}^-]_i$ -sensitivity of WNK1. Furthermore, the pancreatitis-causing R74Q and R75Q mutations in the elbow helix 1 of CFTR hampered WNK1-CFTR physical associations and reduced WNK1-mediated CFTR $P_{\text{HCO}_3^-}/P_{\text{Cl}^-}$ regulation.

CONCLUSION: The CFTR HCO_3^- channel activity is regulated by $[\text{Cl}^-]_i$ and a WNK1-dependent mechanism. Our results provide new insights into the regulation of the ion selectivity of CFTR and the pathogenesis of CFTR-related disorders. (*Cell Mol Gastroenterol Hepatol* 2020;9:79–103; <https://doi.org/10.1016/j.jcmgh.2019.09.003>)

Keywords: Bicarbonate Secretion; Epithelia; Pancreatitis; Ion Selectivity.

Many cystic fibrosis transmembrane conductance regulator (CFTR)-expressing epithelial cells in the gastrointestinal, respiratory, and genitourinary systems and sweat glands secrete and absorb bicarbonate (HCO_3^-)-containing fluids.¹⁻³ HCO_3^- is an essential ingredient in these fluids and performs a wide range of functions. For example, HCO_3^- in the pancreatic juice maintains zymogens in inactive forms within the pancreas, neutralizes gastric acid in the duodenum, and provides an optimum pH environment for digestive enzyme activity in the intestinal lumen.⁴ Moreover, aberrant epithelial HCO_3^- secretion may cause mucin aggregation and mucus plug formation,⁵ which has been hypothesized to underlie the pathogenesis of cystic fibrosis and certain forms of pancreatitis.^{2,6}

In humans, postprandial pancreatic juice contains >140-mM HCO_3^- , indicating that almost all of the anions in the juice are HCO_3^- .⁷ How human pancreatic duct cells secrete fluids that contain such a high HCO_3^- content has long been a puzzle. The identification of critical transporters and their regulatory mechanisms during the last 2 decades has revealed basic principles of pancreatic HCO_3^- secretion. For example, coordination of basolateral HCO_3^- uptake and apical HCO_3^- exit mechanisms by IRBIT plays an important role in agonist-stimulated HCO_3^- secretion in pancreatic ducts.^{8,9} Anion exchangers in the apical membrane of pancreatic duct cells (presumably SLC26A6 and SLC26A3) appear to mediate the apical exit of HCO_3^- during the initial phase of stimulated pancreatic secretion¹⁰; however, as the luminal HCO_3^- concentration increases, HCO_3^- channel activity at the apical membrane is required to maintain the continuous secretion of HCO_3^- and fluids.¹¹ According to the Nernst equation, duct cells can secrete HCO_3^- -rich fluids until the luminal HCO_3^- concentration reaches 200 mM, when the duct cells retain a -60-mV apical membrane potential.¹²

Evidence suggests that CFTR mediates HCO_3^- channel activity at the apical membrane of pancreatic duct cells.^{13,14} The CFTR gene was first identified as a gene associated with cystic fibrosis.¹⁵ CFTR has anion channel activity that conducts anions passively down an electrochemical gradient. Cl^- and HCO_3^- are the most abundant anions in the intracellular and extracellular fluids of animals. Similar to other mammalian anion channels, Cl^- permeates the CFTR channel more readily than HCO_3^- under normal conditions and has a relative HCO_3^- permeability ($P_{\text{HCO}_3^-}/P_{\text{Cl}^-}$) of 0.2-0.4.^{16,17} The CFTR $P_{\text{HCO}_3^-}/P_{\text{Cl}^-}$ is not fixed, however, and can be dynamically modulated by cellular stimuli. For example, a low- $[\text{Cl}^-]_i$ stimulus can increase the CFTR $P_{\text{HCO}_3^-}/P_{\text{Cl}^-}$ to >1 via the activation of $[\text{Cl}^-]_i$ -sensitive kinases.¹⁴ Modeling studies predict that high permeability ($P_{\text{HCO}_3^-}$) and conductance ($G_{\text{HCO}_3^-}$) of bicarbonate via CFTR is essential for generating high bicarbonate flux across duct cells to sustain robust bicarbonate secretion.^{11,18}

Several ion channels and transporters, particularly those transporting Cl^- , are regulated by $[\text{Cl}^-]_i$ -sensitive kinases such as the with-no-lysine kinases (WNKs) and the sterile 20 (STE20)-like kinases. In general, it is believed that WNKs, including WNK1, are initially activated by osmotic stresses, in particular by a decrease in $[\text{Cl}^-]_i$, and

subsequently phosphorylate and activate downstream STE20-like kinases, including oxidative stress-responsive kinase 1 (OSR1) and STE20/SPS1-related proline/alanine-rich kinase (SPAK).¹⁹ Then, the activated STE20-like kinases modulate the activity and cell-surface expression of membrane transport proteins such as the Na^+-Cl^- cotransporters and the $\text{Na}^+-\text{K}^+-\text{Cl}^-$ cotransporters (NKCCs).^{20,21} In the pancreas, the $[\text{Cl}^-]_i$ is ~20 mM in resting ducts cells and falls to ~5 mM during stimulated pancreatic secretion.^{11-13,22} It has been shown that increase in the CFTR $P_{\text{HCO}_3^-}/P_{\text{Cl}^-}$ by $[\text{Cl}^-]_i$ -sensitive kinases is essential for pancreatic HCO_3^- secretion.¹⁴ WNK1 does not affect the $P_{\text{HCO}_3^-}/P_{\text{Cl}^-}$ of the calcium-activated anion channel TMEM16A/ANO1,²³ which implies that WNK1-mediated $P_{\text{HCO}_3^-}/P_{\text{Cl}^-}$ anion channel modulation is not a generalized phenomenon and is potentially specific to CFTR. Notably, defects in CFTR-mediated HCO_3^- channel activity were shown to be associated with pancreatitis and other epithelial disorders.^{6,24} However, the molecular mechanisms by which $[\text{Cl}^-]_i$ -sensitive kinases regulate CFTR anion selectivity and certain CFTR variants increase the risk of epithelial disorders are unknown. Here, we show that physical associations between the N-terminal region of WNK1 and CFTR mediate the $[\text{Cl}^-]_i$ -sensitive regulation of CFTR HCO_3^- permeability and conductance. We also demonstrate that defects in this process underlie the pathogenesis of some CFTR-related disorders by showing that the pancreatitis-causing CFTR mutations R74Q and R75Q⁶ in the elbow helix region hamper the WNK1-CFTR physical association and reduce the WNK1-mediated regulation of CFTR HCO_3^- channel activity.


Results

WNK1 Alone Is Sufficient for the Regulation of CFTR HCO_3^- Permeability and Conductance

We previously showed that activation of the WNK1-SPAK/OSR1 pathway increases the $P_{\text{HCO}_3^-}/P_{\text{Cl}^-}$ of CFTR, which may play a role in pancreatic HCO_3^- secretion.¹⁴ To identify the determinant of WNK1-SPAK/OSR1 signaling, we first examined the effects of single and combinatorial expressions of these kinases on CFTR $P_{\text{HCO}_3^-}/P_{\text{Cl}^-}$. The relative anion permeability was measured using whole-cell recording of human CFTR expressed in HEK293T cells

*Authors share co-first authorship.

Abbreviations used in this paper: CFTR, cystic fibrosis transmembrane conductance regulator; E_{rev} , reversal potential; GFP, green fluorescent protein; GST, glutathione S-transferase; HCO_3^- , bicarbonate; IBMX, 3-isobutyl-1-methylxanthine; I-V, current-voltage; MD, molecular dynamics; NKCC, $\text{Na}^+-\text{K}^+-\text{Cl}^-$ cotransporter; NL, N-linker; NMDG, N-methyl-D-glucamine; OSR1, oxidative stress-responsive kinase 1; $P_{\text{HCO}_3^-}/P_{\text{Cl}^-}$, $\text{HCO}_3^-/\text{Cl}^-$ permeability ratio; PKA, protein kinase A; P_o , open probability; PRD, proline-rich domain; SDS, sodium dodecyl sulfate; siRNA, small interfering RNA; SPAK, STE20/SPS1-related proline/alanine-rich kinase; STE20, sterile 20; WNK1, with-no-lysine kinase 1; WT, wild-type.

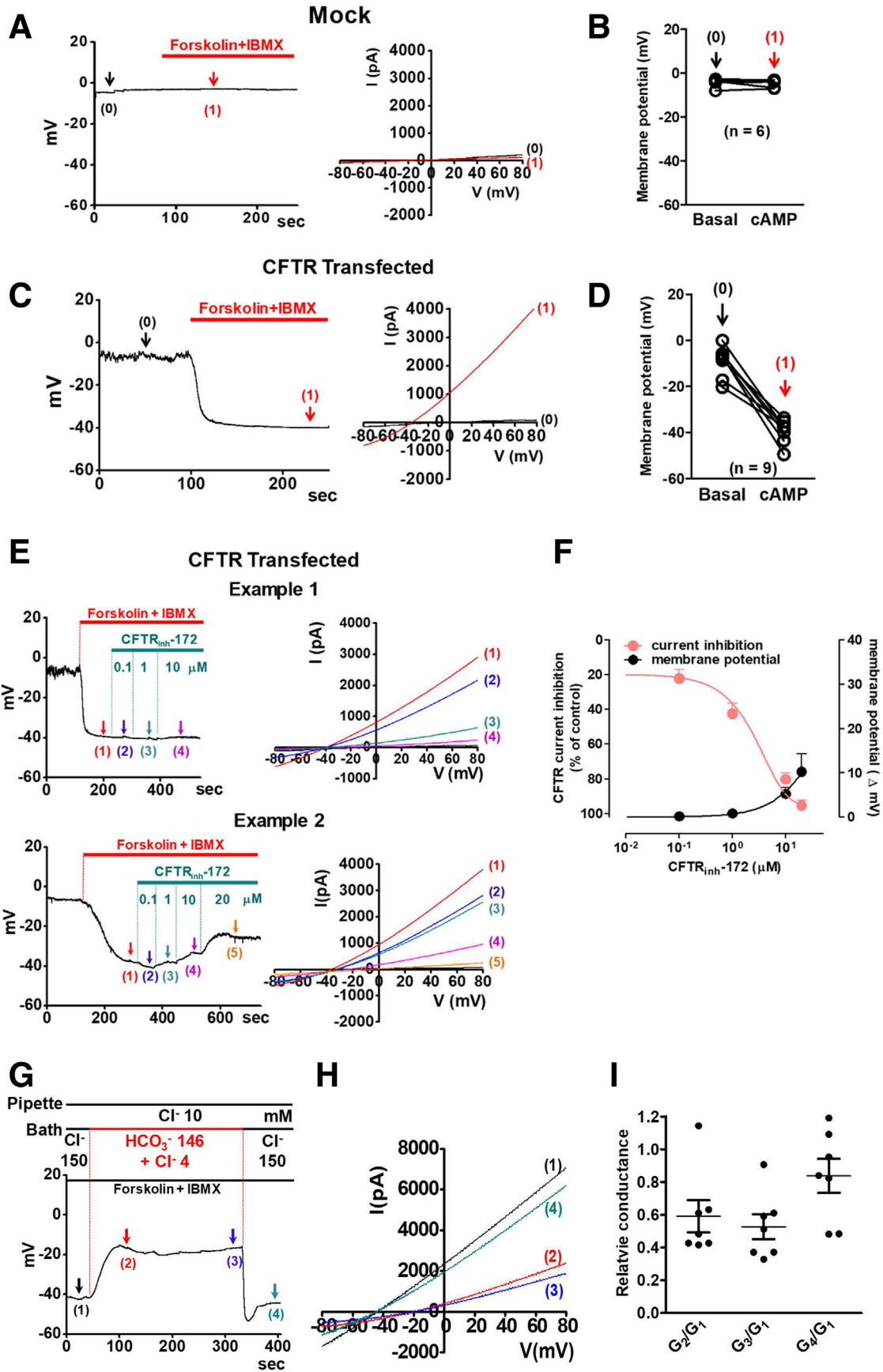
 Most current article

© 2020 The Authors. Published by Elsevier Inc. on behalf of the AGA Institute. This is an open access article under the CC BY-NC-ND license (<http://creativecommons.org/licenses/by-nc-nd/4.0/>).

2352-345X

<https://doi.org/10.1016/j.jcmgh.2019.09.003>

Pipette: 10 mM Cl⁻, Bath: 150 mM Cl⁻



with coexpression of WNK1, SPAK, or OSR1 (Figures 1–3). To activate the WNK1-SPAK/OSR1 pathway, the pipette solution contained a low concentration of Cl^- (10 mM). As shown in Figure 1A–D, cAMP stimulation of CFTR-expressing HEK293T cells evoked an anion current, which induced a negative shift in the membrane potential due to the influx of Cl^- . Notably, current reductions of up to 80% did not greatly affect membrane potentials. The conductance levels of background currents (G_{BG}) were 0.2–0.5 nS and those of cAMP-activated CFTR currents (G_{CFTR}) were 10–30 nS. Inhibition of CFTR currents by 83% with the CFTR inhibitor, CFTR_{inh}-172 (10 μM), increased the ratio of the background currents to the CFTR currents ($G_{\text{BG}}/G_{\text{CFTR}}$) from approximately 0.02 to 0.10, which caused a subtle change in membrane potential (<5 mV, corresponding to <0.1 in $P_{\text{HCO}_3^-}/P_{\text{Cl}^-}$) (Figure 1E and F). These data indicated that background or leak currents did not significantly affect the results in membrane potential measurements (see also Discussion).

In Figure 1G, the replacement of bath solutions with a HCO_3^- -rich solution evoked membrane depolarization, indicating that CFTR $P_{\text{HCO}_3^-}$ is smaller than P_{Cl^-} , and an average of 41% reduction in anion conductance, indicating that CFTR $G_{\text{HCO}_3^-}$ is smaller than G_{Cl^-} under control conditions. During a 6-minute whole-cell recording, the membrane potential was not altered by a partial rundown (up to 17%) of the anion conductance (Figure 1G–I).

Representative whole-cell recording with coexpression of WNK1, SPAK, and OSR1 are shown in Figure 2A–H (zero-current clamp) and Figure 3 (current-voltage [I–V] relationship). A summary of the $P_{\text{HCO}_3^-}/P_{\text{Cl}^-}$ values from the zero-current clamp recordings is presented in Figure 2I. As reported previously,¹⁴ CFTR $P_{\text{HCO}_3^-}/P_{\text{Cl}^-}$ is significantly increased by WNK1-SPAK or WNK-OSR1 under the low- $[\text{Cl}^-]_i$ condition (Figures 2A–C and 3A–C). In contrast to the known regulation of Na^+ - Cl^- cotransporters or NKCC that requires downstream STE20-like kinases (SPAK or OSR1),^{19,20} the expression of WNK1 alone increased CFTR $P_{\text{HCO}_3^-}/P_{\text{Cl}^-}$ under low- $[\text{Cl}^-]_i$ conditions (Figures 2D and 3D). Furthermore, expression of SPAK and OSR1 did not affect

CFTR $P_{\text{HCO}_3^-}/P_{\text{Cl}^-}$ (Figures 2E–G and 3E–G; a summary in Figure 2H). The WNK1 effect occurred in cells in which endogenous SPAK and OSR1 were silenced, further indicating that SPAK and OSR1 are not required for CFTR regulation and that WNK1 alone is sufficient for upregulation of CFTR $P_{\text{HCO}_3^-}/P_{\text{Cl}^-}$ (Figures 2H and 3H). The immunoblot results shown in Figure 2J verified the proper expression and silencing of SPAK and OSR1 in the experiments. Of interest, WNK1 increased not only HCO_3^- permeability, but also HCO_3^- conductance ($G_{\text{HCO}_3^-}$) of CFTR (Figure 4). The surface biotinylation data indicated that neither depletion nor overexpression of WNK1 significantly altered the cell-surface expression of CFTR in HEK293T cells (Figure 5). These results suggest that WNK1 regulates CFTR HCO_3^- permeability and conductance by modulating the anion channel properties rather than altering CFTR stability or trafficking.

WNK1 N-Terminal Region Is Critical for the Upregulation of CFTR $P_{\text{HCO}_3^-}/P_{\text{Cl}^-}$

We next examined the effects of WNK1 on CFTR using truncated WNK1 proteins to identify the critical domains that regulate CFTR $P_{\text{HCO}_3^-}/P_{\text{Cl}^-}$ (Figures 6 and 7). WNK1 is a large protein composed of 2126 amino acids (Figure 8A).²⁵ Plasmids expressing the N-terminal proline-rich domain (PRD) [WNK1(1–119)], PRD + N-linker (NL) [WNK1(1–221)], kinase domain [WNK1(221–491)], PRD + NL + kinase domain [WNK1(1–491)], or the remaining C-terminal regions [WNK1(492–2126)] were co-transfected in HEK293T cells, and CFTR $P_{\text{HCO}_3^-}/P_{\text{Cl}^-}$ was analyzed by measuring whole-cell current. Figures 6A–G and 7 show representative zero-current clamp recording and I–V measurements, respectively. Figure 6H shows a summary of the $P_{\text{HCO}_3^-}/P_{\text{Cl}^-}$ values from zero-current clamp recordings. The expression of the WNK1 N-terminal regions [WNK1(1–491)] (Figures 6F and 7F), and particularly that of the kinase domain [WNK1(221–491)] alone (Figure 6E and 7E), increased the CFTR $P_{\text{HCO}_3^-}/P_{\text{Cl}^-}$, whereas that of the remaining C-terminal regions [WNK1(492–2126)] did not (Figure 6G and 7G).

Figure 1. (See previous page). **Measurements of CFTR Cl^- and HCO_3^- channel activities in control cells.** (A–D) The cAMP-activated Cl^- current was measured in HEK293T cells transfected with (A, B) mock or (C, D) CFTR-expressing plasmids. Representative voltage and current measurements are shown in panels A and C) and a summary of voltage measurements is presented in panels B and D). The pipette and bath solutions contained 10-mM Cl^- and 150-mM Cl^- , respectively. CFTR currents were activated by cAMP (5- μM forskolin and 100- μM IBMX) after whole-cell configuration was established. To determine the I–V relationship during zero-current clamp recordings, the clamp mode was shifted to the voltage clamp mode, and an I–V curve was obtained by applying ramp pulses. Arrows indicate the time point to measure I–V curve. (A, B) The cAMP stimulation evoked no discernible voltage and current changes in mock transfected cells ($n = 6$). (C, D) The same cAMP treatment evoked a Cl^- current in CFTR-expressing cells, which induced a negative shift of membrane potential due to the influx Cl^- ($n = 9$). (E, F) The cAMP-activated CFTR current was measured in HEK293T cells after treatment with the CFTR inhibitor, CFTR_{inh}-172. Two examples of sample traces, showing the minimum (Example 1) and maximum (Example 2) voltage change by CFTR_{inh}-172, are shown in panel E. A summary of voltage and current change by CFTR_{inh}-172 is presented in panel F. (G, H) CFTR currents were activated by 5- μM forskolin and 100- μM IBMX. The pipette and bath solutions contained 10-mM Cl^- . The initial bath solution containing 150-mM Cl^- was replaced with a solution containing 146-mM HCO_3^- and 4-mM Cl^- . Replacing bath solutions with a HCO_3^- -rich solution (G) evoked a membrane depolarization and (H) reductions in anion conductance of CFTR. (I) A summary of slope conductance data is shown ($n = 7$). Replacing bath solutions with a HCO_3^- -rich solution evoked a 41% reduction in anion conductance (G_2/G_1). During a 6-minute whole-cell recording, cells retained over 83% of CFTR Cl^- conductance (G_4/G_1) and membrane potentials were not altered [compare points (1) and (4) in panel G]. Data are presented as the mean \pm SEM.

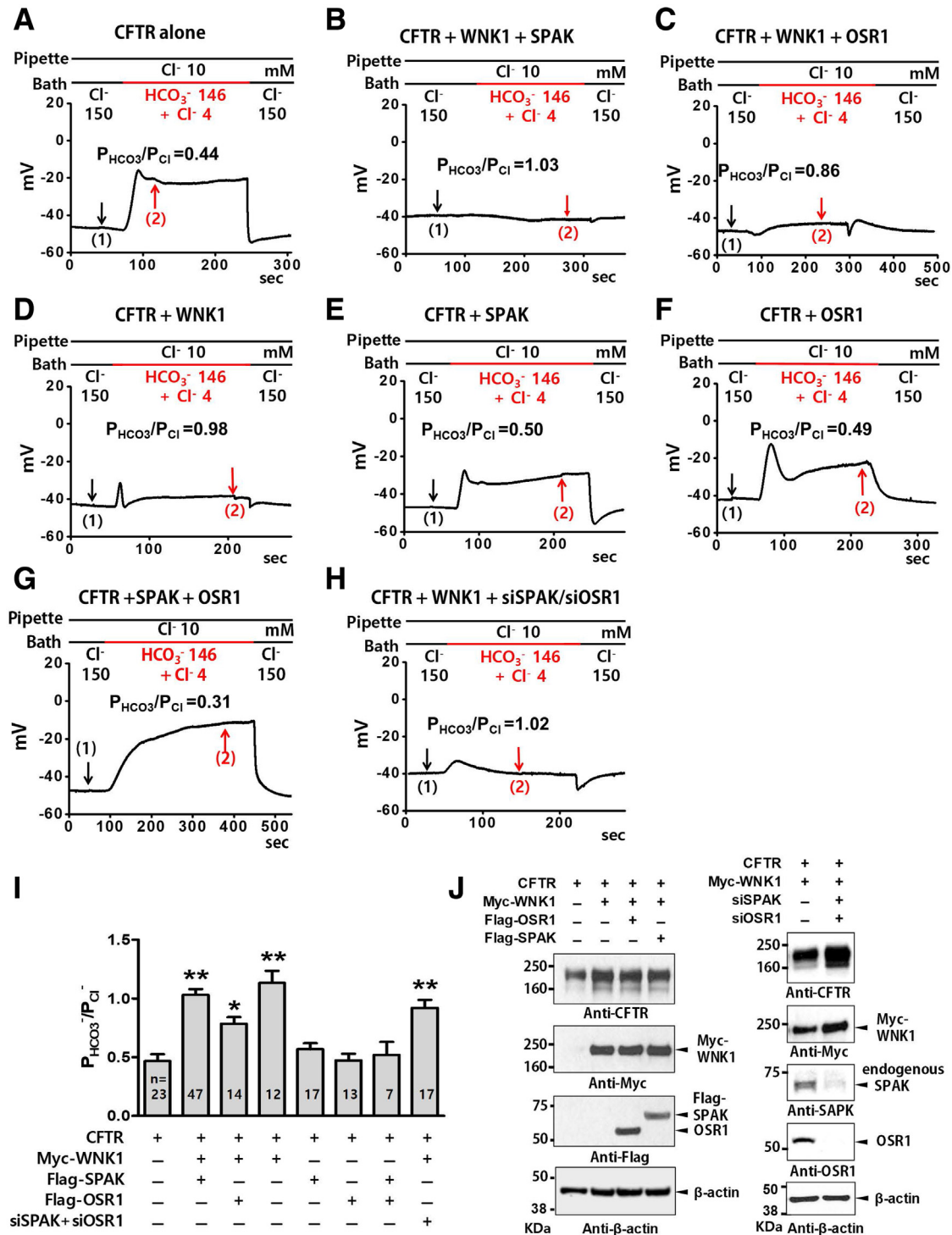


Figure 2. WNK1 alone is sufficient to regulate CFTR HCO_3^- permeability. (A–I) The relative HCO_3^- permeability ($P_{\text{HCO}_3^-}/P_{\text{Cl}^-}$) of CFTR was analyzed using HEK293T cells transfected with plasmids expressing CFTR, Myc-WNK1, Flag-OSR1, Flag-SPAK, or siRNAs against SPAK and OSR1. Whole-cell currents were measured after the activation of CFTR channels by cAMP (5- μM forskolin and 100- μM IBMX). The initial bath solution containing 150-mM Cl^- was replaced with a solution containing 4-mM Cl^- and 146-mM HCO_3^- . Representative voltage measurements are shown in A–H, and a summary of $P_{\text{HCO}_3^-}/P_{\text{Cl}^-}$ values from the zero-current clamp recording is presented in panel I. To determine the current-voltage (I–V) relationship during zero-current clamp recordings, the clamp mode was shifted to the voltage clamp mode, and an I–V relationship was obtained by applying ramp pulses (Figure 3, arrows indicate the time points that were used to measure the I–V relationship). Bar-graph data are presented as the mean \pm SEM. * $P < .05$, ** $P < .01$: difference from CFTR alone. (J) Expression of CFTR, WNK1, OSR1, and SPAK was analyzed by immunoblotting. HEK293T cells transiently transfected with plasmids containing CFTR, Myc-WNK1, Flag-SPAK, and Flag-OSR expressed proteins with the appropriate molecular weights (left panel). siRNAs against SPAK and OSR1 abolished endogenous expression of SPAK and OSR1 (right panel). The β -actin blot represents the housekeeping loading control. Four independent experiments displayed similar results.

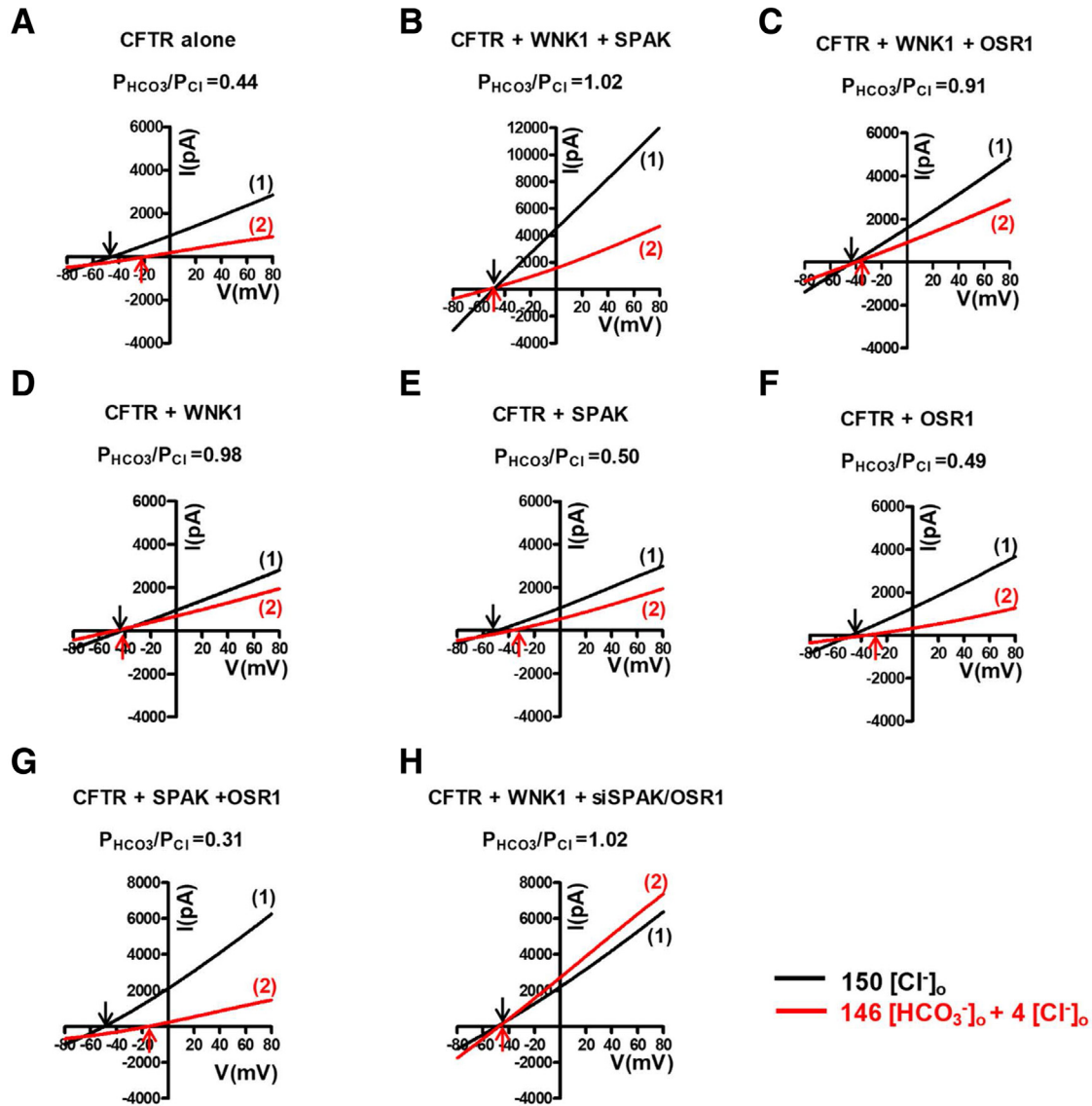


Figure 3. I-V relationship for the whole-cell current measurements in Figure 2A-H. (A-H) The I-V relationship was measured at each time point marked in the corresponding panels of Figure 2A-H. The I-V relationship was measured at each time point marked in the corresponding panels of Figure 2A-H. The $P_{\text{HCO}_3^-}/P_{\text{Cl}^-}$ of CFTR was analyzed using HEK293T cells transfected with plasmids expressing CFTR, Myc-WNK1, Flag-OSR1, Flag-SPAK, or siRNAs against SPAK and OSR1. To determine the I-V relationship during zero-current clamp recordings, the clamp mode was shifted to the voltage clamp mode, and the I/V curve was obtained by applying ramp pulses from -80 mV to 80 mV (0.8 -mV/ms holding potential, near the resting membrane potential). The I/V curves were analyzed in the initial bath solution containing 150 -mM Cl^- (1) and in a solution containing 4 -mM Cl^- and 146 -mM HCO_3^- (2). Each reversal potential is marked with an arrow. WNK1 alone is sufficient for the upregulation of the CFTR $P_{\text{HCO}_3^-}/P_{\text{Cl}^-}$.

To understand the molecular basis of CFTR $P_{\text{HCO}_3^-}/P_{\text{Cl}^-}$ modulation via WNK1, we then examined the physical association between CFTR and the truncated WNK1 proteins using a semi pull-down assay (Figure 8). Cell lysates taken from CFTR-expressing HEK293T cells were incubated with recombinant glutathione S-transferase (GST)-tagged WNK1 proteins in media containing high (150 mM) and low (0 mM) Cl^- concentrations and the amount of CFTR protein bound to each truncated WNK1 was analyzed. Of interest, the WNK1 kinase domain [WNK1(221–491)] associated strongly with CFTR regardless of the Cl^- concentration. The inclusion of the regions surrounding the kinase domain,

including the WNK1 auto-inhibitory domain and a coiled-coil domain [WNK1(1–665)], greatly reduced the binding to CFTR in the high- Cl^- (150 mM) medium but not in the low- Cl^- (0 mM) medium, suggesting that Cl^- inhibits the physical association between WNK1 and CFTR through these WNK1 regions. Collectively, these results imply that the WNK1 N-terminal region mediates the upregulation of CFTR $P_{\text{HCO}_3^-}/P_{\text{Cl}^-}$ via a $[\text{Cl}^-]_i$ -dependent physical association with CFTR.

Because the kinase domain is critical for the upregulation of the CFTR $P_{\text{HCO}_3^-}/P_{\text{Cl}^-}$ (Figures 6 and 7) and for the physical association between WNK1 and CFTR (Figure 8),

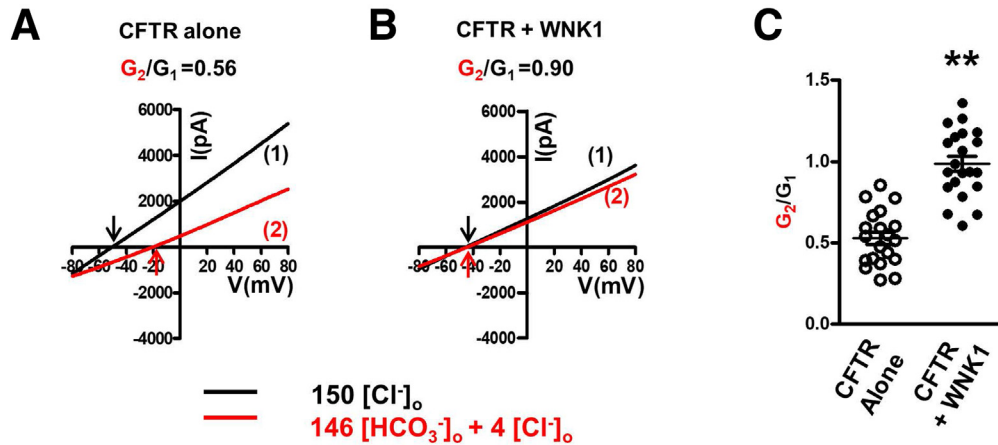


Figure 4. WNK1 increases the bicarbonate conductance ($G_{\text{HCO}_3^-}$) of CFTR. (A) In cells expressing CFTR alone, changing bath solutions from a Cl^- -rich solution (1) to a HCO_3^- -rich solution (2) evoked reductions in anion channel conductance. (B) In cells coexpressing WNK1, replacing bath solutions with a HCO_3^- -rich solution did not significantly reduce the slope conductance. (C) A summary of results showed that WNK1 increased the HCO_3^- conductance ($G_{\text{HCO}_3^-}$) of CFTR, when normalized to each Cl^- current ($G_{\text{HCO}_3^-}/G_{\text{Cl}^-}$, G_2/G_1 , $n = 20$ for CFTR alone and $n = 21$ for CFTR + WNK1). Data are presented as the mean \pm SEM. $**P < .01$.

we investigated whether the WNK1 kinase activity is involved in CFTR regulation (Figures 9 and 10) using a kinase-dead WNK1(D368A) mutant that is catalytically inactive and does not phosphorylate downstream SPAK and OSR1.²⁶ Of note, the kinase-dead D368A mutation did not

abolish the WNK1 effect on the upregulation of CFTR $P_{\text{HCO}_3^-}/P_{\text{Cl}^-}$ (Figures 9A and 10A; see summary in Figure 9H). In addition, the WNK1(D368A) mutant retained the ability to bind to CFTR at low $[\text{Cl}^-]_i$ (Figure 9J). A recent crystallographic study identified a Cl^- -sensing region in the WNK1

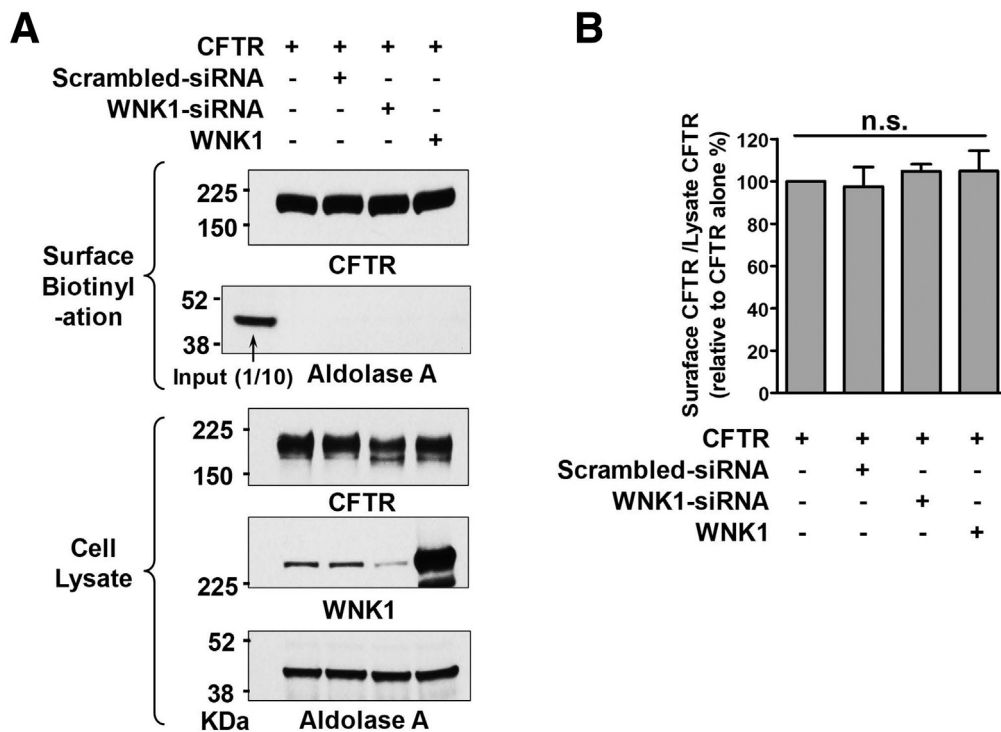


Figure 5. Surface expression of CFTR with depletion or overexpression of WNK1 in HEK293 cells. HEK293T cells were transfected with plasmids expressing WT CFTR and (1) scrambled RNA, (2) siRNA against WNK1, or (3) WNK1 plasmids, and the surface biotinylation assays were performed. Representative immunoblots are shown in panel A and a summary of multiple experiments are shown in panel B ($n = 5$). Cell surface-specific labelling of proteins was confirmed by the absence of the cytosolic protein aldolase A in the biotinylated fraction. Neither depletion nor overexpression of WNK1 significantly altered the cell-surface expression of CFTR. n.s., not significant.

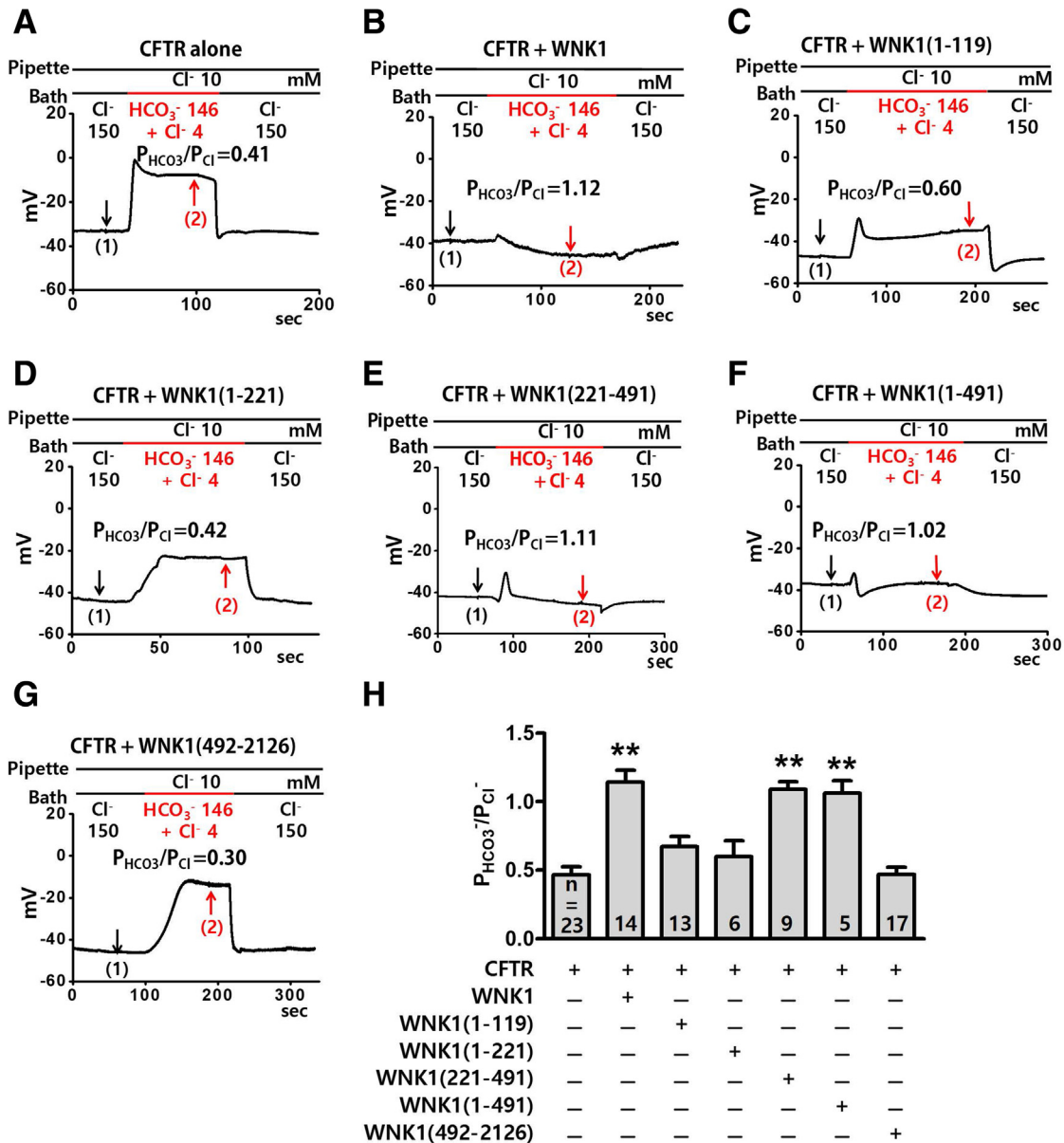


Figure 6. The WNK1 kinase domain is critical for the upregulation of CFTR HCO₃⁻ permeability. (A–G) The $P_{\text{HCO}_3^-}/P_{\text{Cl}^-}$ of CFTR was analyzed in HEK293T cells transfected with plasmids containing the WNK1 N-terminal PRD [WNK1(1–119)], PRD + NL [WNK1(1–221)], kinase domain [WNK1(221–491)], PRD + NL + kinase domain [WNK1(1–491)], and the remaining C-terminal regions [WNK1(492–2126)]. The domain structure of human WNK1 is depicted in Figure 8A. Whole-cell currents were measured after the activation of CFTR channels by cAMP (5- μ M forskolin and 100- μ M IBMX) using the same protocol used in Figure 2. Representative voltage measurements are shown. To determine the I-V relationship during zero-current clamp recordings (Figure 7, arrows indicate the time points used to measure the I-V relationship). (H) A summary of the $P_{\text{HCO}_3^-}/P_{\text{Cl}^-}$ values from zero-current clamp recordings is presented. Truncated WNK1 proteins containing the kinase domain [WNK1(221–491) and WNK1(1–491)] increased the CFTR $P_{\text{HCO}_3^-}/P_{\text{Cl}^-}$. Bar-graph data are presented as the mean \pm SEM. ** $P < .01$: difference from CFTR alone.

kinase domain (L369, G370, and L371), in which Cl⁻ binding prevents kinase autophosphorylation and activation.¹⁹ The WNK1-L369F/L371F mutant has repeatedly been used to induce Cl⁻-insensitive constitutive activation of WNK1-kinase activity.²⁷ Mutagenesis of this region (L369F, L371F, and L369F/L371F) did not affect the WNK1-mediated regulation of CFTR $P_{\text{HCO}_3^-}/P_{\text{Cl}^-}$ (Figures 9B–D and 10B–D) or the low [Cl⁻]_i-induced association between

WNK1 and CFTR (Figure 9). It has been shown that the GXXXP motif in some proteins, such as NBCe1-B and NBCe2-C, functions as an intracellular Cl⁻ sensor.²⁸ The WNK1 N-terminal region contains 2 putative GXXXP sites (G14A/P18A and G274A/P278A); therefore, we examined their functional significance. Single or double mutations in the 2 GXXXP sites did not affect CFTR $P_{\text{HCO}_3^-}/P_{\text{Cl}^-}$ regulation (Figures 9E–G and 10E–G). WNK1 association with CFTR

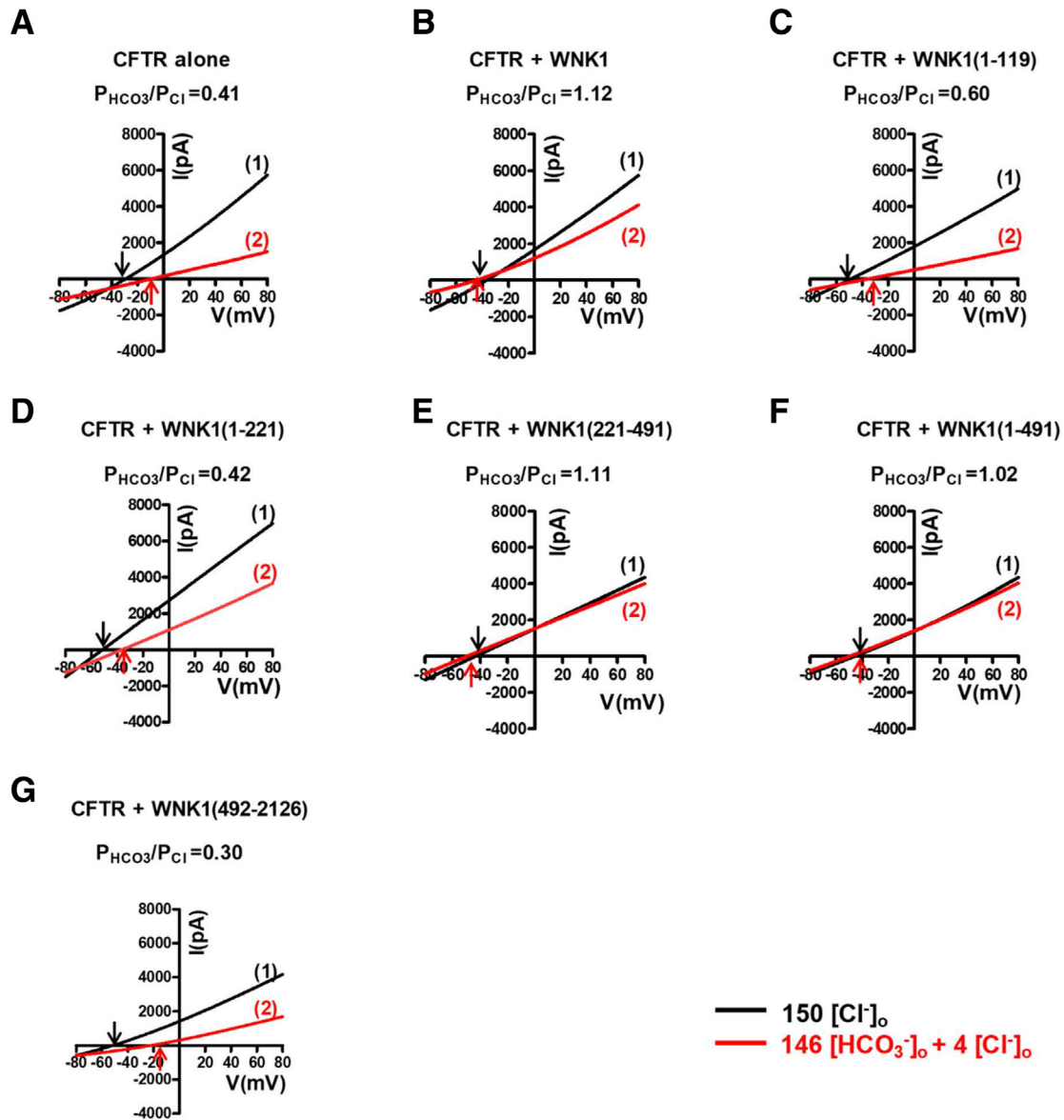


Figure 7. Current/voltage (I/V) relationship for the whole-cell current measurements in Figure 6A–G. (A–G) The I–V relationship was measured at each time point marked in the corresponding panels of Figure 6A–G. The $P_{\text{HCO}_3^-}/P_{\text{Cl}^-}$ of CFTR was analyzed in HEK293T cells expressing truncated WNK1 proteins. To determine the current–voltage relationship during zero-current clamp recordings, the clamp mode was shifted to the voltage clamp mode, and the I/V curve was obtained by applying ramp pulses from -80 mV to 80 mV (0.8 mV/ms holding potential, near the resting membrane potential). The I/V curves were analyzed in the initial bath solution containing 150 -mM Cl^- (1) and in a solution containing 4 -mM Cl^- and 146 -mM HCO_3^- (2). Each reversal potential is marked an arrow. Truncated WNK1 proteins containing the kinase domain [WNK1(221–491) and WNK1(1–491)] increased the CFTR $P_{\text{HCO}_3^-}/P_{\text{Cl}^-}$.

was also unaffected by mutations in the putative GXXXX sites (Figure 9). Taken together, these results suggest that WNK1 kinase activity and its known Cl^- -binding sites are not involved in the regulation of CFTR $P_{\text{HCO}_3^-}/P_{\text{Cl}^-}$.

WNK1 N-Terminal Region Modulates the Ion Selectivity of CFTR in Excised Patch Clamp Recordings

Bi-ionic potential measurements based on whole-cell recordings might contain erroneous signals, in particular,

due to potential ion depletion or accumulation.²⁹ To minimize this problem, we measured the CFTR $P_{\text{HCO}_3^-}/P_{\text{Cl}^-}$ in excised patch clamp configurations using recombinant WNK1 proteins. Although the kinase domain [WNK1(221–491)] alone was sufficient to increase the CFTR $P_{\text{HCO}_3^-}/P_{\text{Cl}^-}$ in whole-cell recordings (Figures 6 and 7) and for the association of WNK1 with CFTR in pull-down assays (Figure 8), the recombinant WNK1(221–491) protein tended to form precipitates in patch solutions. Therefore, we performed the excised patch recordings using the recombinant protein containing the WNK1 N-terminal regions

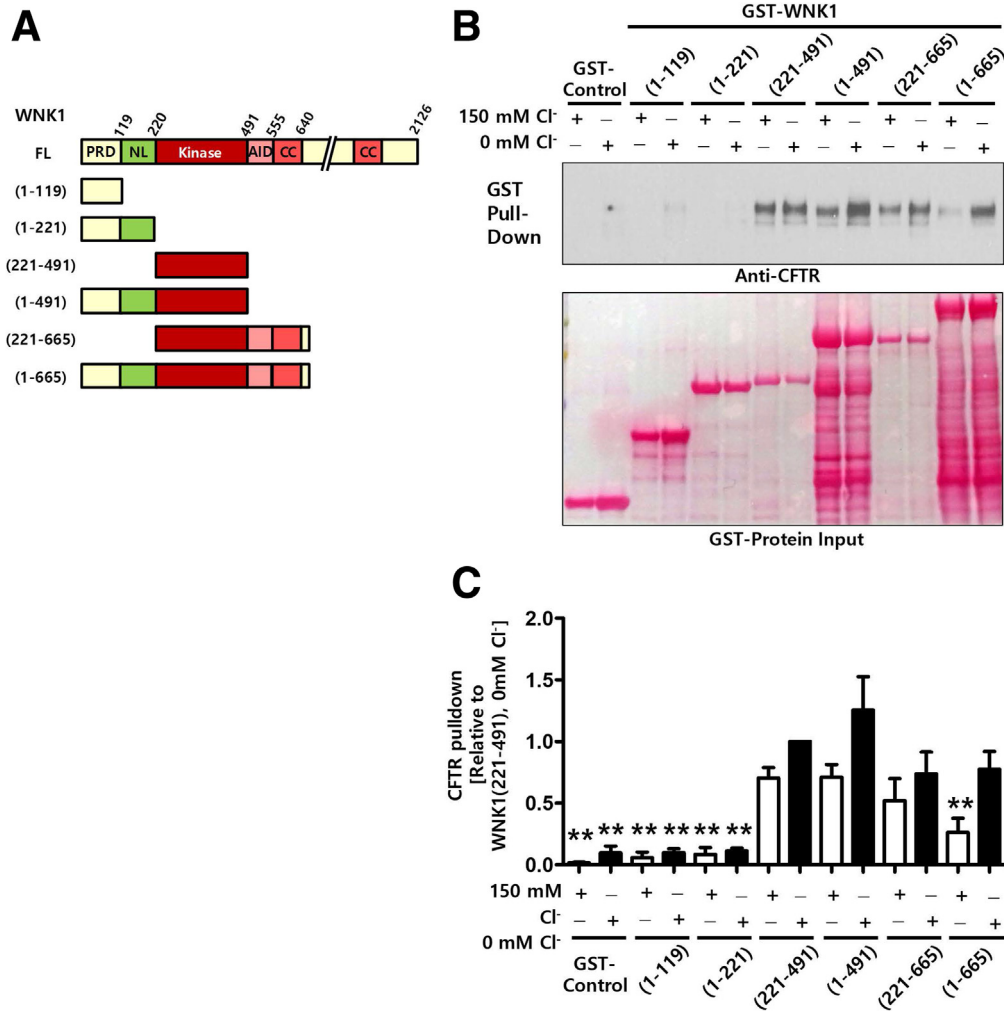


Figure 8. The WNK1 N-terminal region interacts with CFTR in a $[Cl^-]_i$ -dependent manner. (A) Schematic diagram of the WNK1 constructs used in pull-down assays. (B, C) Semi-pull-down assays were performed with recombinant GST-WNK1 fragments and cell lysates prepared from HEK293T cells expressing CFTR. GST pull-down assays were done in Cl^- -free and high- Cl^- (150 mM) media. Representative blots are shown in panel B, and a summary of CFTR pull-down values relative to WNK1(221-491) protein at 0-mM Cl^- is illustrated in panel C, $n = 4$). The kinase domain of WNK1 strongly binds to CFTR regardless of Cl^- concentration. The inclusion of regions surrounding the kinase domain [WNK1(1-665)] reduces the WNK1-CFTR interaction in 150-mM Cl^- medium. Error bars are presented as the mean \pm SEM. $**P < .01$: difference from WNK1(221-491) at 0-mM Cl^- . AID, auto-inhibitory domain; CC, coiled-coil domain; FL, full-length; KD, kinase domain.

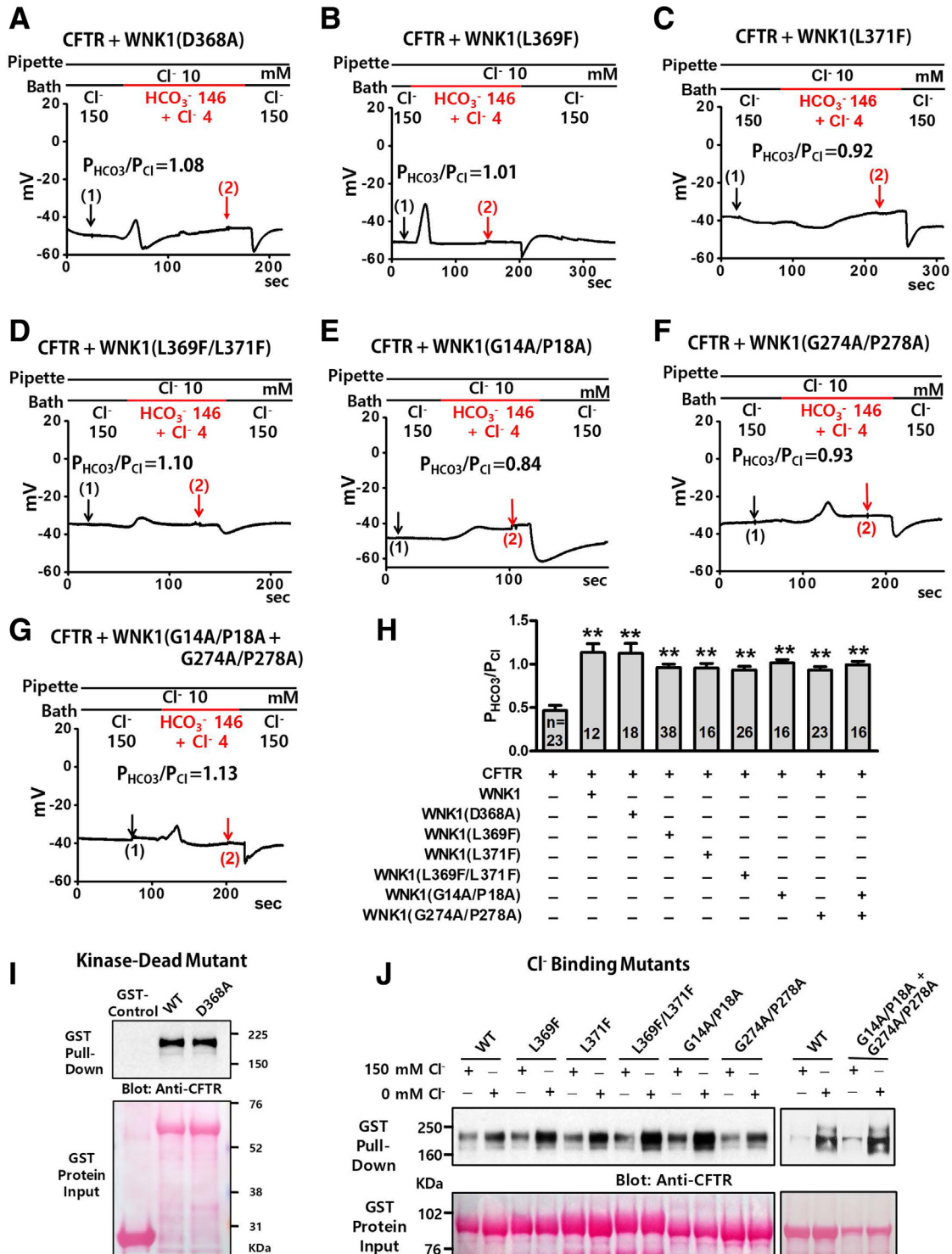
[WNK1(1-491)], which was chemically stable in all of the experimental solutions. WNK1(1-491) showed Cl^- -sensitive binding to CFTR with an IC_{50} value of 10.1 mM $[Cl^-]$, and 84% of maximum CFTR binding activity was retained at a 4-mM Cl^- concentration (Figure 11). In outside-out patch clamp recordings, the addition of WNK1(1-491) to the intracellular side of the pipette solution increased the CFTR $P_{HCO_3^-}/P_{Cl^-}$ (Figure 12A-C), recapitulating the findings of the whole-cell recordings. More remarkably, the addition of WNK1(1-491) to the bath solution (intracellular side) in inside-out patch clamp recordings increased the CFTR $P_{HCO_3^-}/P_{Cl^-}$ in a dose-dependent manner (Figure 12D-F). The EC_{50} value of WNK1(1-491) that was required for the CFTR $P_{HCO_3^-}/P_{Cl^-}$ increase was 3.2 μ M (95% confidence interval, 2.3-4.2 μ M) at 10-mM $[Cl^-]_i$ and shifted to 1.1 μ M (95% confidence interval, 0.2-2.0 μ M) at 4-mM $[Cl^-]_i$, indicating

that the EC_{50} value was left-shifted and the WNK1 effect was augmented at lower $[Cl^-]_i$ (Figure 12F).

An increase in the $P_{HCO_3^-}/P_{Cl^-}$ of some anion channels is associated with increases in the pore size and the dielectric constant (ϵ) of the selectivity filter.¹⁶ Because the WNK1 N-terminal region increased the CFTR $P_{HCO_3^-}/P_{Cl^-}$ (Figures 6 and 12), we next examined whether WNK1(1-491) increased the pore size and ϵ of the CFTR selectivity filter (Figure 13). Inside-out recordings with control GST and WNK1(1-491) proteins showed that WNK1(1-491) increased the CFTR $P_{HCO_3^-}/P_{Cl^-}$, whereas the addition of GST did not (Figure 13A-C). The ion selectivity of most anion channels is principally determined by a combination of the pore size (area exclusion) effect and the anion transfer free-energy (dehydration-energy) effect. It has been shown that the area exclusion effect dominantly affects I^- permeation through the CFTR channel because of the large size

of the I⁻ ion compared with the size of the CFTR functional pore.¹⁶ On the other hand, the dehydration-energy effect mainly determines NO₃⁻ permeation, because NO₃⁻ is a medium-sized, symmetrically charged ion. Accordingly, the CFTR I⁻ permeability is reported to be less than the CFTR Cl⁻ permeability because of a large area exclusion effect, while the CFTR NO₃⁻ permeability is greater than the CFTR Cl⁻

permeability because of a small dehydration-energy penalty.^{16,30} Similar to previous reports,^{16,30} the relative permeability of I⁻ (P_I/P_{Cl}) was only 0.59 ± 0.04 in our inside-out recordings. Notably, this value was increased to 0.84 ± 0.04 by WNK1(1-491) (Figure 13D-F), suggesting an increase in the CFTR pore size, which relieves the energy barrier of area exclusion. We next examined the effect of WNK1(1-491) on



NO_3^- permeability. The relative NO_3^- permeability ($P_{\text{NO}_3^-}/P_{\text{Cl}^-}$) was 1.92 ± 0.17 under the control condition and was reduced to 1.42 ± 0.08 by WNK1(1–491) (Figure 13G–I), indicating an increase in the pore size of CFTR, which increases the ϵ of the CFTR selectivity filter and thus relieves the dehydration-energy penalty difference between NO_3^- and Cl^- . These results imply that the WNK1 N-terminal region modulates the ion selectivity of CFTR by increasing the size of the CFTR functional pore.

Next, we examined the effects of WNK1(1–491) on CFTR channel conductance using inside-out configurations (Figure 14). Macroscopic CFTR currents were measured in symmetrically Cl^- -rich (150 Cl^-) and HCO_3^- -rich (146 $\text{HCO}_3^- + 4 \text{Cl}^-$) solutions. Notably, addition of WNK1(1–491) to the bath (intracellular side) increased CFTR HCO_3^- conductance ($G_{\text{HCO}_3^-}$) by $76 \pm 13\%$ ($n = 9$) (Figure 14C and D), whereas the same WNK1(1–491) did not affect the CFTR Cl^- conductance (G_{Cl^-}) (Figure 14A and B).

Effects of WNK1 on CFTR Single-Channel Activity

We analyzed the effects of WNK1 on CFTR single-channel activity to confirm the permeability and conductance changes observed in whole-cell and macroscopic excised patch recordings. Representative inside-out patch traces and I-V measurements are shown in Figure 15A–D, and the summarized results are presented in Figure 15E–H. WNK1 did not significantly affect the single-channel activity of the CFTR Cl^- current, including the single-channel conductance and open probability (P_o) (Figure 15A, B, and E–H). Changing the bath (intracellular) side to a HCO_3^- -rich solution evoked a +32 mV shift of reversal potential ($P_{\text{HCO}_3^-}/P_{\text{Cl}^-} = 0.25$). Importantly, the addition of 10- μM WNK1(1–491) to the bath induced a negative shift of reversal potential leading to +14 mV ($P_{\text{HCO}_3^-}/P_{\text{Cl}^-} = 0.56$), which again indicates a WNK1-induced increase in $P_{\text{HCO}_3^-}/P_{\text{Cl}^-}$ (Figure 15D). Of interest, WNK1 also increased single-channel conductance, P_o , and the open dwell time of CFTR HCO_3^- currents (Figure 15E–H).

Molecular Pathogenic Mechanisms of CFTR Mutations Associated With Pancreatitis

A recent study indicated that 9 CFTR mutants that impair WNK1-regulated HCO_3^- permeation are associated with pancreatitis, rhinosinusitis, and male infertility.⁶ To

understand the molecular basis of these pathogenic CFTR mutants, we first examined the ability of CFTR mutants to bind WNK1 using a semi-pull-down assay. Two CFTR mutations, R74Q and R75Q, located in the N-terminal “elbow helix” region caused significant reductions in the WNK1-CFTR association (Figure 16A and B). Defects in the WNK1-CFTR association, as well as intrinsic defects in the CFTR channel pore, can impair the WNK1-regulated HCO_3^- permeation of CFTR. We chose R74Q and L997F as representative mutations that induce defects in the CFTR HCO_3^- channel by WNK1-related and nonrelated mechanisms, respectively. We then performed inside-out patch recordings with WNK1(1–491). In macroscopic current analyses, the EC_{50} value of WNK1(1–491) that was required for increased CFTR $P_{\text{HCO}_3^-}/P_{\text{Cl}^-}$ at 4 mM $[\text{Cl}^-]_i$ was 0.7 μM (95% confidence interval, 0.2–1.2 μM) in the control wild-type (WT) CFTR, and this value was right-shifted to 2.9 μM (95% confidence interval, 1.8–4.1 μM) in the CFTR R74Q mutant (Figure 16C–E). On the other hand, WNK1(1–491) at concentrations up to 10 μM did not increase CFTR $P_{\text{HCO}_3^-}/P_{\text{Cl}^-}$ in the CFTR L997F mutant (Figure 16C and F). These results support the notion that R74Q impairs the regulated HCO_3^- permeation of CFTR by inhibiting WNK1-CFTR association, while L997F causes other intrinsic defects in the CFTR pore that impede HCO_3^- permeation.

Discussion

Cl^- and HCO_3^- are the 2 most abundant anions that can be the charge carrier of CFTR, although diverse anions permeate through the anion channels of animal cells. Therefore, changes in CFTR HCO_3^- permeability and conductance that determine the amount of HCO_3^- flux across the apical membrane of CFTR-expressing epithelia have important physiological and pathological implications. Our integrated molecular and physiological approach revealed that the N-terminal region of WNK1 senses $[\text{Cl}^-]_i$ and regulates CFTR $P_{\text{HCO}_3^-}/P_{\text{Cl}^-}$ by physically associating or dissociating with CFTR. Whole-cell, outside-out, and inside-out patch clamp studies indicated that WNK1 fragments containing the kinase domain are sufficient for modulating the ion selectivity and conductance of CFTR. Pull-down assays with recombinant WNK1 fragments showed that the WNK1 kinase domain physically interacts with CFTR and

Figure 9. (See previous page). WNK1 kinase activity and known Cl^- -binding sites are not involved in the upregulation of CFTR HCO_3^- permeability. (A–H) The $P_{\text{HCO}_3^-}/P_{\text{Cl}^-}$ of CFTR was analyzed in HEK293T cells expressing WNK1 mutant proteins. Plasmids expressing the kinase-dead WNK1 mutant (D368A) and WNK1 mutants bearing mutations in the putative Cl^- -binding regions of the kinase domain (L369F, L371F, and L369F/L371F) and GXXX motifs (G14A/P18A, G274A/P278A, and double mutant G14A/P18A/G274A/P278A) were co-transfected. Whole-cell currents were measured after the activation of CFTR channels by cAMP (5- μM forskolin and 100- μM IBMX) using the same protocol used in Figure 2. Representative voltage and current measurements are shown in panels A–G and Figure 10 (arrows indicate the time points that were used to measure I-V relationship). A summary of the $P_{\text{HCO}_3^-}/P_{\text{Cl}^-}$ values from zero-current clamp recordings is presented in panel H. Bar-graph data are presented as the mean \pm SEM. **** $P < .01$:** difference from CFTR alone. WNK1 mutants exhibited no statistical difference when compared to WT WNK1. (I) Semi pull-down assays were performed with recombinant GST-WNK1(221–491) bearing the kinase-dead D368A mutation and cell lysates prepared from HEK293T cells expressing CFTR under the 0-mM Cl^- condition. Three independent experiments displayed similar results. (J) Semi pull-down assays were performed with recombinant GST-WNK1(1–491) bearing mutations in the putative Cl^- -binding regions and cell lysates prepared from HEK293T cells expressing CFTR under the 0-mM and 150-mM Cl^- conditions. Three independent experiments displayed similar results.

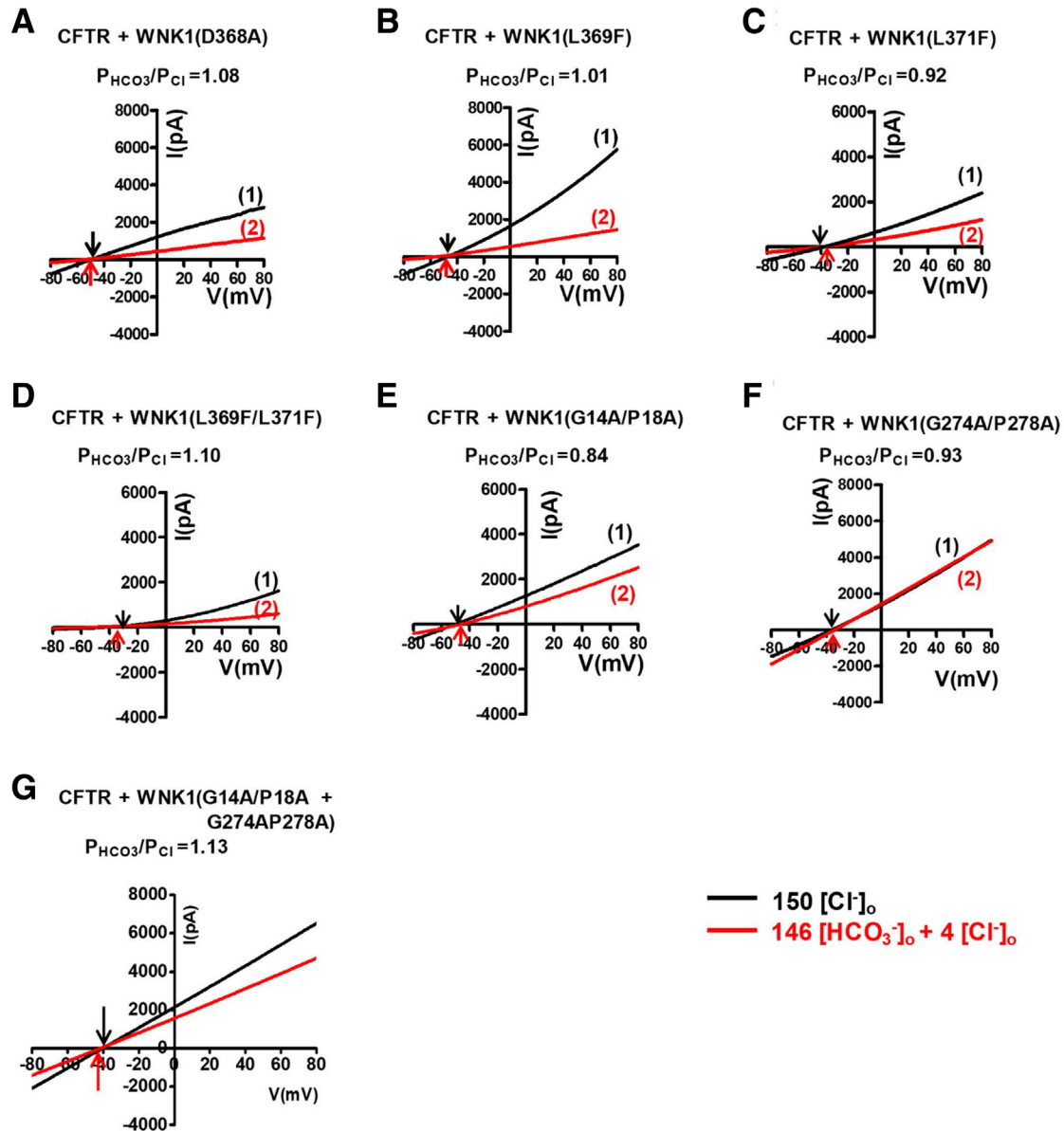


Figure 10. Current/voltage (I/V) relationship for the whole-cell current measurements in Figure 9A–G. (A–G) The I–V relationship was measured at each time point marked in the corresponding panels of Figure 9A–G. The $P_{\text{HCO}_3^-}/P_{\text{Cl}^-}$ of CFTR was analyzed in HEK293T cells expressing the kinase-dead WNK1 mutant (D368A) and WNK1 mutants bearing mutations in the putative Cl^- -binding regions of the kinase domain (L369, G370, and L371) and GXXX motifs (G14A/P18A and G274A/P278A). To determine the current-voltage relationship during zero-current clamp recordings, the clamp mode was shifted to the voltage clamp mode, and the I/V curve was obtained by applying ramp pulses from -80 mV to 80 mV (0.8 mV/ms holding potential, near the resting membrane potential). The I/V curves were analyzed in the initial bath solution containing 150 -mM Cl^- (1) and in a solution containing 4 -mM Cl^- and 146 -mM HCO_3^- (2). Each reversal potential is marked with an arrow. The kinase-dead D368A mutation and mutations in the known Cl^- -binding sites of WNK1 did not affect the ability of WNK1 to upregulate the CFTR $P_{\text{HCO}_3^-}/P_{\text{Cl}^-}$.

that the surrounding N-terminal regions inhibit the WNK1–CFTR association in a Cl^- -dependent manner.

A notable finding in the present study is that the WNK1 kinase domain, but not its kinase activity, is involved in the regulation of CFTR ion selectivity. In many cases, WNKs regulate membrane transport proteins by phosphorylating downstream STE20-like kinases such as OSR1 and SPAK.³¹ In those cases, intact kinase activity is critical for the regulation of the membrane transporters, and the loss of the

kinase activity abolishes the WNK-mediated regulation. However, in the present study, the kinase-dead WNK1 D368A mutation did not affect the ability of WNK1 to upregulate CFTR $P_{\text{HCO}_3^-}/P_{\text{Cl}^-}$ (Figure 9). This result is compatible with the finding that STE20-like kinases are not required for CFTR regulation (Figure 2). It has been suggested that WNKs regulate the expression and function of some transporters via a kinase activity-independent mechanism.^{32,33} For example, multiple intramolecular and

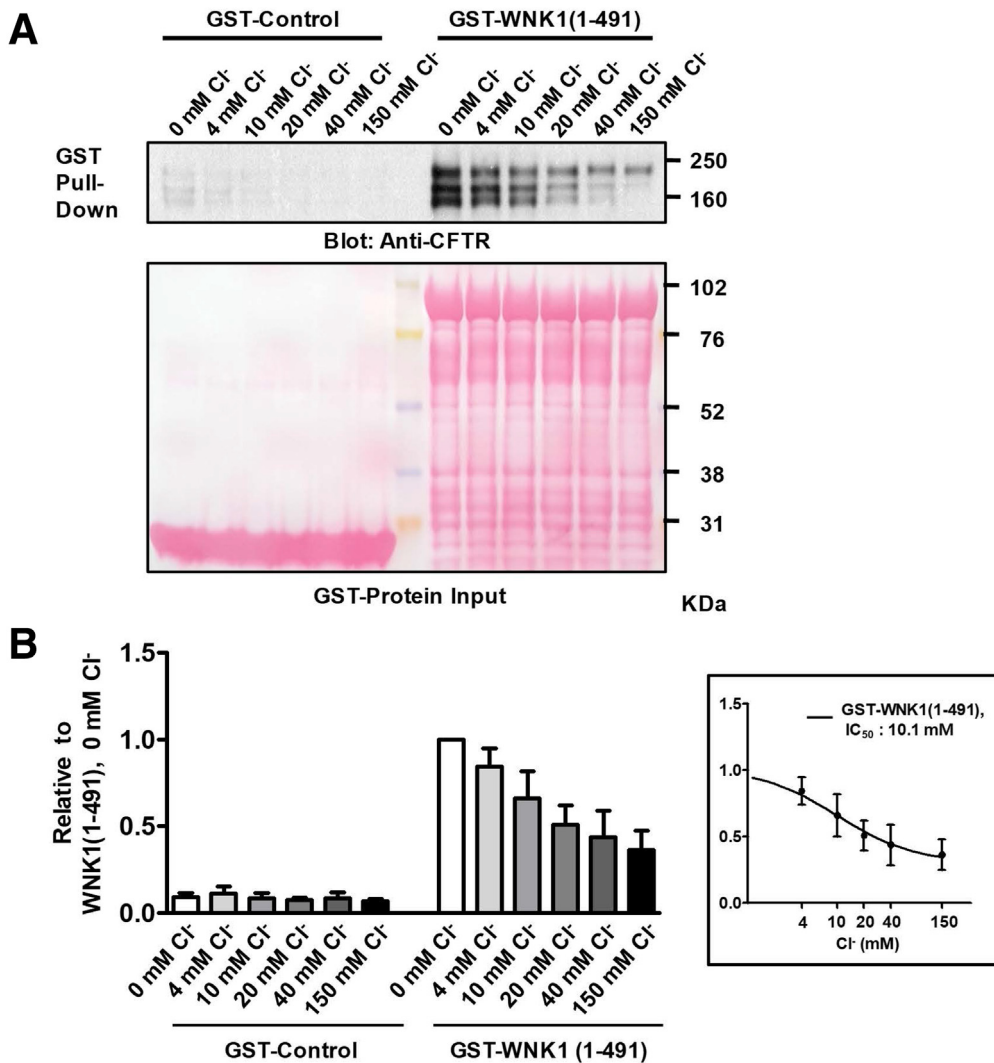


Figure 11. CFTR-WNK1 pull-down assays at various Cl⁻ concentrations. Semi pull-down assays were performed with recombinant GST-WNK1 fragments and cell lysates prepared from CFTR-expressing HEK293T cells. GST pull-down assays were done at various Cl⁻ concentrations (0, 4, 10, 20, 40, and 150 mM) by replacing Cl⁻ with gluconate (see Methods). Representative blots are shown in panel A, and a summary of CFTR pull-down values (n = 7) relative to WNK1(1–491) protein at 0-mM Cl⁻ is illustrated in panel B. The IC₅₀ value of [Cl⁻] that inhibits the binding between GST-WNK1(1–491) and CFTR was calculated as 10.1-mM (B, inset). Data are presented as mean ± SEM.

intermolecular interactions of the WNK1 N-terminal regions, including the kinase domain, mediate the inhibition of ROMK1 via a noncatalytic mechanism.²⁵ In addition, the WNK kinase activity is not required for the WNK/SPAK-mediated regulation of NBCe1-B.³⁴ Taken together with the present results for CFTR, the noncatalytic but kinase domain-dependent mechanism of regulation appears to be one of the general mechanisms by which WNKs regulate target proteins.

A crystallographic study of the recombinant WNK1 kinase domain identified a Cl⁻ binding site within the kinase domain where Cl⁻ binding inhibits the catalytic activation of WNK1.¹⁹ Mutations at this site (L369F, L371F, and L369F/L371F) affected neither the ability of WNK1 to regulate the CFTR P_{HCO₃}/P_{Cl} nor the [Cl⁻]_i-dependent association of WNK1 with CFTR (Figure 9). These results are in agreement with the idea that WNK1 regulates CFTR ion selectivity via a noncatalytic mechanism and suggest that the [Cl⁻]_i-dependence of the association between WNK1 and CFTR is not related to the kinase activity. Our results indicate that the

overall [Cl⁻]_i-dependence of the effects of WNK1 on CFTR originates from potential Cl⁻-sensing sites in the PRD + NL (aa. 1–221) and auto-inhibitory domain + first coiled-coil (aa. 492–665) regions (Figure 8). The binding of Cl⁻ to these regions appears to induce structural changes that inhibit the physical association between the WNK1 kinase domain and CFTR.

The precise WNK1-binding sites of CFTR need to be addressed in future studies. Experiments with pancreatitis-causing CFTR mutants revealed that R74 and R75, located in the first elbow helix region of CFTR, are critically involved in the WNK1-CFTR association (Figure 16). Notably, a computational protein-protein docking analysis using the Protein Data Bank-deposited structures of hCFTR,³⁵ zebrafish CFTR in the phosphorylated, adenosine triphosphate (ATP)-bound conformation,³⁵ and the WNK1 kinase domain³⁶ showed that WNK1 S231–T234 and I384–E388 potentially bind to intracellular hCFTR regions near R74–R75 (Figure 17). According to a 3.9-Å cryo-EM structure of human CFTR, the handle-like first elbow helix is

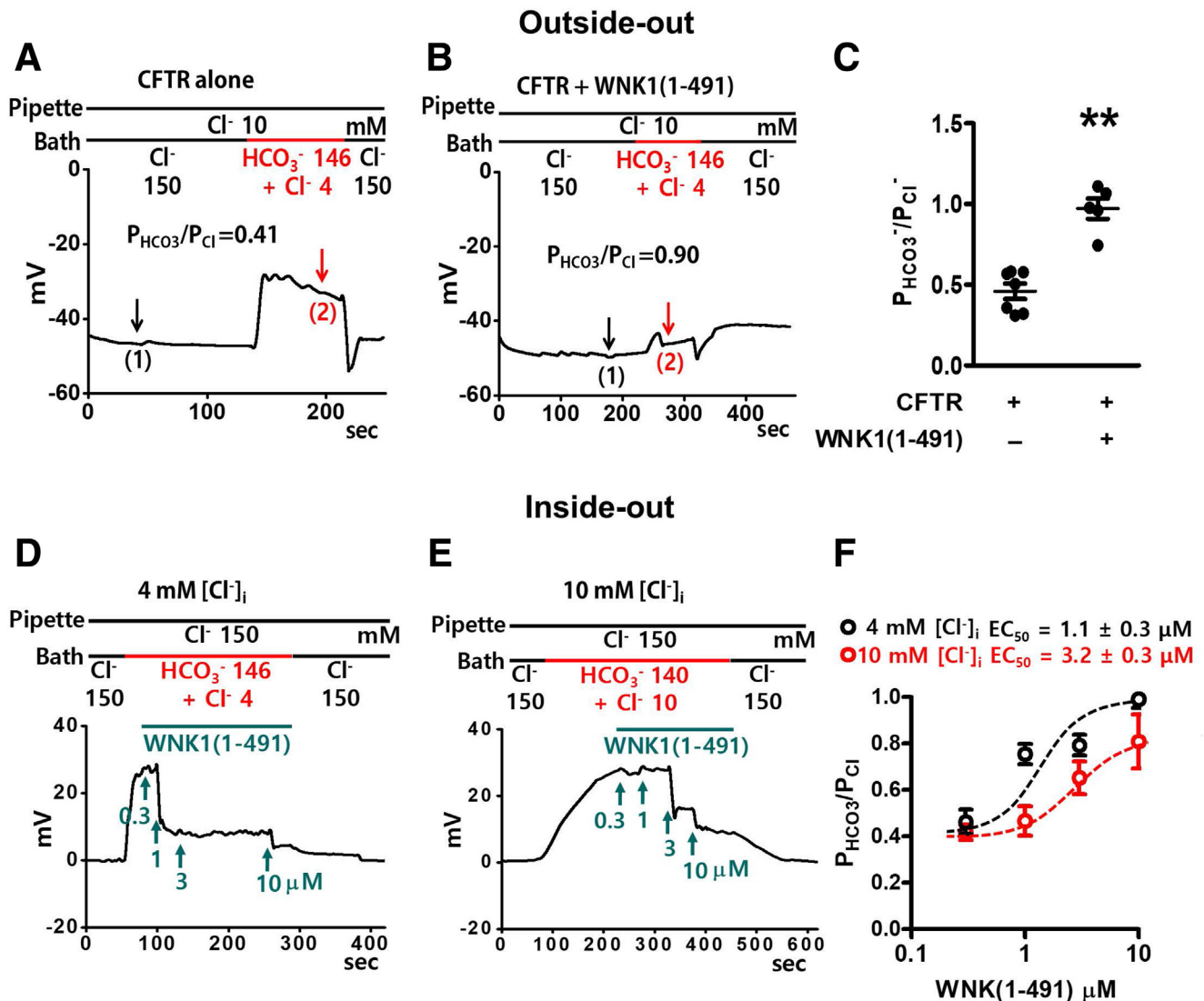


Figure 12. Measurements of CFTR $P_{\text{HCO}_3^-}/P_{\text{Cl}^-}$ in excised patch clamp recordings using recombinant WNK1 proteins. (A–C) The membrane potential was measured in outside-out patch clamp recordings using patch membranes prepared from HEK293T cells expressing CFTR. The low- Cl^- (10 mM) pipette solution contained the catalytic subunit of protein kinase A (PKA, 10 U/mL) and 3-mM MgATP to activate CFTR. The addition of recombinant WNK1(1–491) (3 μM) to the pipette solution increased the CFTR $P_{\text{HCO}_3^-}/P_{\text{Cl}^-}$. Representative voltage measurements are shown in panels A and B and a summary of $P_{\text{HCO}_3^-}/P_{\text{Cl}^-}$ values from zero-current clamp recordings is presented in panel C. Data are presented as the mean \pm SEM (CFTR alone; $n = 7$ and CFTR+WNK1 (1–491); $n = 5$). $**P < .01$: difference from CFTR alone. (D–F) Membrane potential was measured in inside-out patch clamp recordings using patch membranes prepared from HEK293T cells expressing CFTR. The low- Cl^- (4 mM or 10 mM) bath solution (intracellular side) contained the catalytic subunit of protein kinase A (PKA, 10 unit/mL) and 3-mM MgATP to activate CFTR. The addition of recombinant WNK1(1–491) (1 ~ 10 μM) to the bath solution increased the CFTR $P_{\text{HCO}_3^-}/P_{\text{Cl}^-}$ in a dose-dependent manner. (F) The dose-response curve was left-shifted at 4-mM $[\text{Cl}^-]_i$, the relationship of the $P_{\text{HCO}_3^-}/P_{\text{Cl}^-}$ values from zero-current clamp recordings and WNK1 (1–491) is presented. Data are presented as the mean \pm SEM ($n = 7$).

located immediately ahead of transmembrane domain 1 and contacts a proximally located lasso motif that has been suggested to play a role in CFTR gating and regulation of the R domain.³⁵ Taken together, it appears that the binding of WNK1 to this CFTR region favors the open structure of the CFTR pore to facilitate HCO_3^- permeation.

An increase in the pore diameter of anion channels increases the $P_{\text{HCO}_3^-}/P_{\text{Cl}^-}$ by alleviating the energy barrier of area exclusion and, more importantly, by reducing the dehydration-energy penalty due to an increase in the ϵ of

the pore region.¹⁶ Results in Figure 13 support the notion that WNK1 may increase the CFTR anion channel pore diameter. In addition to the reductions in the energy barriers of area exclusion and dehydration, CFTR channel-specific factors seem to be involved in the WNK1-induced increase in CFTR $P_{\text{HCO}_3^-}/P_{\text{Cl}^-}$. We frequently observed that WNK1 stimulation caused CFTR $P_{\text{HCO}_3^-}/P_{\text{Cl}^-}$ to reach values >1 . Simple reductions in the energy barrier of area exclusion and the difference in dehydration penalty between HCO_3^- and Cl^- can only explain increases in the CFTR

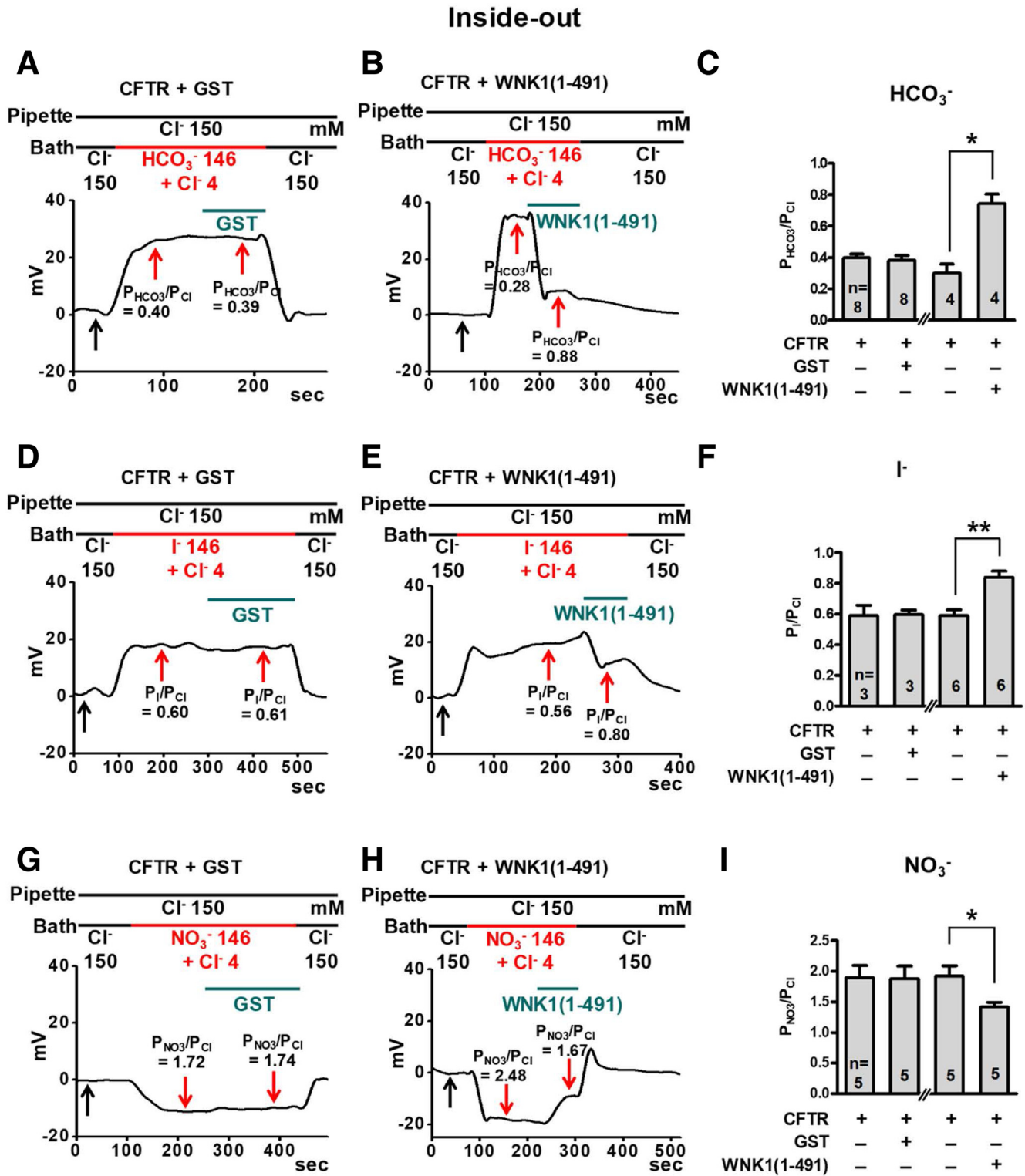


Figure 13. Measurements of CFTR P_x/P_{Cl} and P_{NO₃⁻}/P_{Cl} in inside-out patch clamp recordings with recombinant WNK1 proteins. The membrane potential was measured in inside-out patch clamp recordings using patch membranes prepared from HEK293T cells expressing CFTR. The low-Cl⁻ (4 mM) bath solution (intracellular side) contained the catalytic subunit of PKA (10 U/mL) and 3-mM MgATP to activate CFTR. The CFTR P_{HCO₃⁻}/P_{Cl} (A-C), P_I/P_{Cl} (D-F), and P_{NO₃⁻}/P_{Cl} (G-I) values were analyzed with changing ionic compositions of the bath solution using a protocol as detailed in the Materials and Methods section. The addition of recombinant WNK1(1-491) (3 μM) to the bath solution increased P_I/P_{Cl} and reduced P_{NO₃⁻}/P_{Cl}. Representative voltage measurements are shown in panels A, B, D, E, G, and H, and summaries of the respective P_x/P_{Cl} values from zero-current clamp recordings are presented in panels C, F, and I, respectively. Bar graph data are presented as the mean ± SEM. *P < .05, **P < .01: difference from CFTR alone.

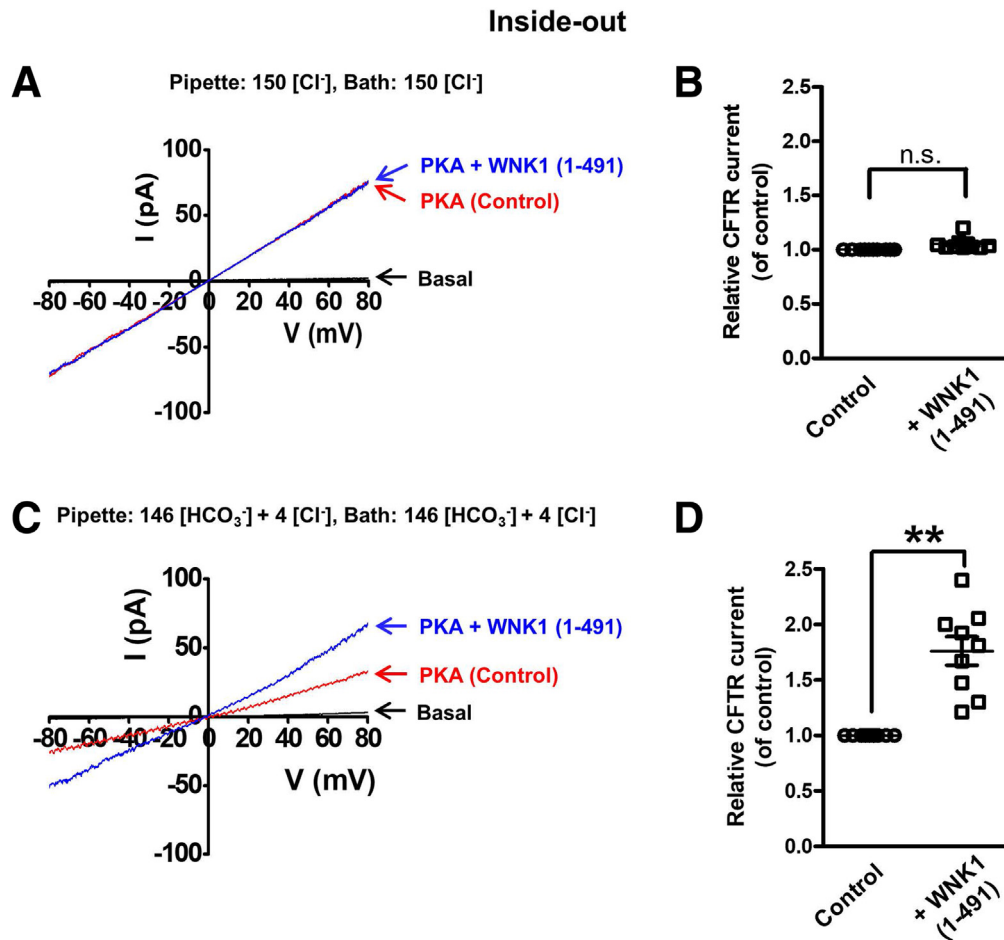


Figure 14. Measurements of CFTR conductance in inside-out patch clamp recordings with recombinant WNK1 proteins. (A, B) Macroscopic currents were recorded from inside-out membrane patches using symmetrically Cl^- -rich (150 mM) solutions in CFTR-expressing HEK293T cells. Patch membranes were prepared from HEK293T cells expressing CFTR. CFTR currents were activated by addition of the catalytic subunit of protein kinase A (PKA, 10 unit/mL) to a 3-mM MgATP containing bath solution (intracellular side). The I-V relationship was obtained by applying ramp pulses from -80 to $+80$ mV (0.8 mV/ms) at resting state (basal) and after additions of PKA (Control) and PKA + WNK1(1-491) to the bath solution. Representative traces are shown in panel A and a summary of relative CFTR currents at -60 mV (normalized by control G_{Cl}) are shown in panel B ($n = 10$). (C, D) Macroscopic CFTR currents were recorded from inside-out membrane patches using symmetrically HCO_3^- -rich (146 HCO_3^- + 4 Cl^-) solutions. The I-V relationship was obtained at resting state (basal) and after additions of PKA (Control) and PKA + WNK1(1-491) to the bath solution. Representative traces are shown in panel C and a summary of relative CFTR currents (normalized by control G_{HCO_3}) are shown in panel D ($n = 9$). Data are presented as the mean \pm SEM. ****** $P < .05$: difference from CFTR alone.

$P_{\text{HCO}_3}/P_{\text{Cl}}$ up to a value of 1. Therefore, other factors that favor the permeation of HCO_3^- should play a role in the mechanism by which WNK1 increases the CFTR $P_{\text{HCO}_3}/P_{\text{Cl}}$ to values >1 . Another interesting finding, the mechanism of which needs to be examined in future studies, is the increase in the conductance and P_o of CFTR HCO_3^- channel. Increase in CFTR G_{HCO_3} as well as $P_{\text{HCO}_3}/P_{\text{Cl}}$ has paramount importance in augmenting HCO_3^- flux across the apical membrane of epithelial cells.^{3,11,37} According to the dielectric tunnel theory of anion selectivity, anions that exhibit higher permeability may have a decreased conductance because they bind more tightly in the channel.³⁸ However, in the present study, the CFTR HCO_3^- permeability increase is not coupled with the HCO_3^- conductance decrease. Collectively, these findings indicate that WNK1 exerts complex

effects on CFTR HCO_3^- channel activity in addition to pore dilation.

In the present study, excised cell-free patch experiments revealed that WNK1 affects the ion selectivity of CFTR in a dose-dependent and $[\text{Cl}^-]_i$ -dependent manner (Figure 12D-F). Measurements of the bi-ionic potentials using whole-cell recordings might contain erroneous results because of the series resistance and ion depletion/accumulation problems.²⁹ Importantly, inside-out and outside-out patch experiments (Figure 12), in which the ion depletion or accumulation problems are minimal, produced results comparable to those of whole-cell recordings (Figures 2 and 6). Furthermore, we used a zero-current clamping mode to measure the membrane potentials during whole-cell recordings and used those values for all

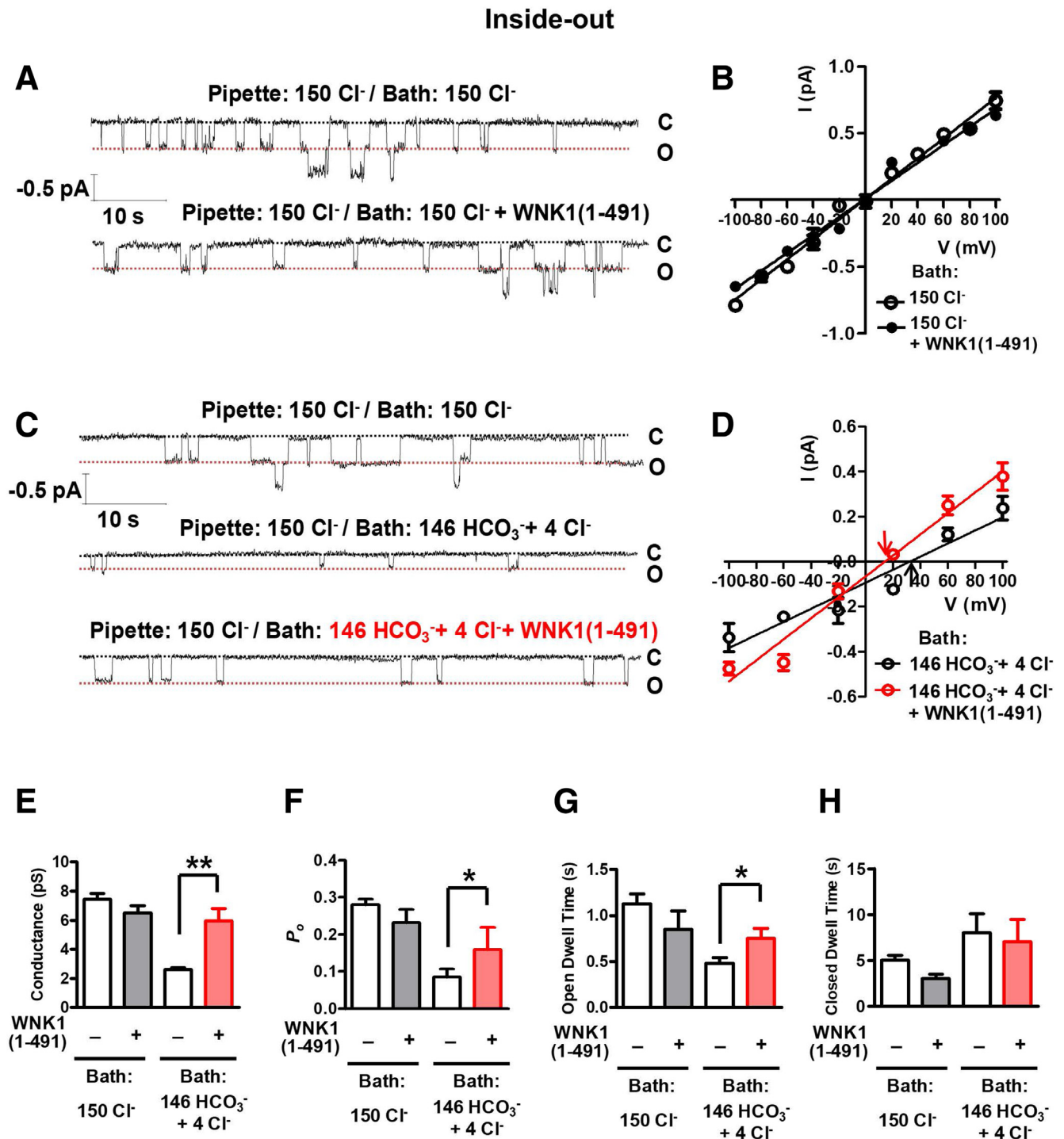


Figure 15. Effects of WNK1 on CFTR single-channel activity. (A, B) Single-channel current recordings were performed in excised, inside-out patches in HEK293T cells with addition of WNK1(1-491) (10 μ M). Representative (A) inside-out patch traces and (B) I-V measurements with a 150-mM Cl⁻-containing solution in the bath (intracellular) side. (C, D) Representative (C) inside-out patch traces and (D) I-V measurements in which the bath side was changed to a HCO₃⁻-rich solution. Arrows indicate E_{rev}. (E-H) A summary of single-channel conductance (E), open probability (P_o, F), open dwell time (G), and closed dwell time (H) (n = 10 for Bath 150-mM Cl⁻, n = 9 for Bath 146-mM HCO₃⁻ + 4-mM Cl⁻). Bar-graph data are presented as the mean \pm SEM. *P < .05, **P < .01.

mechanistic analyses, which will minimize the potential change problems caused by series resistance.³⁹ Last, reductions in CFTR anion channel conductance may alter membrane potential when the recorded currents are

contaminated with considerable amounts of background or leak currents. However, as shown in Figure 1, up to 50% inhibition of G_{CFTR} showed no discernible changes in membrane potential. Therefore, an \sim 50% reduction of

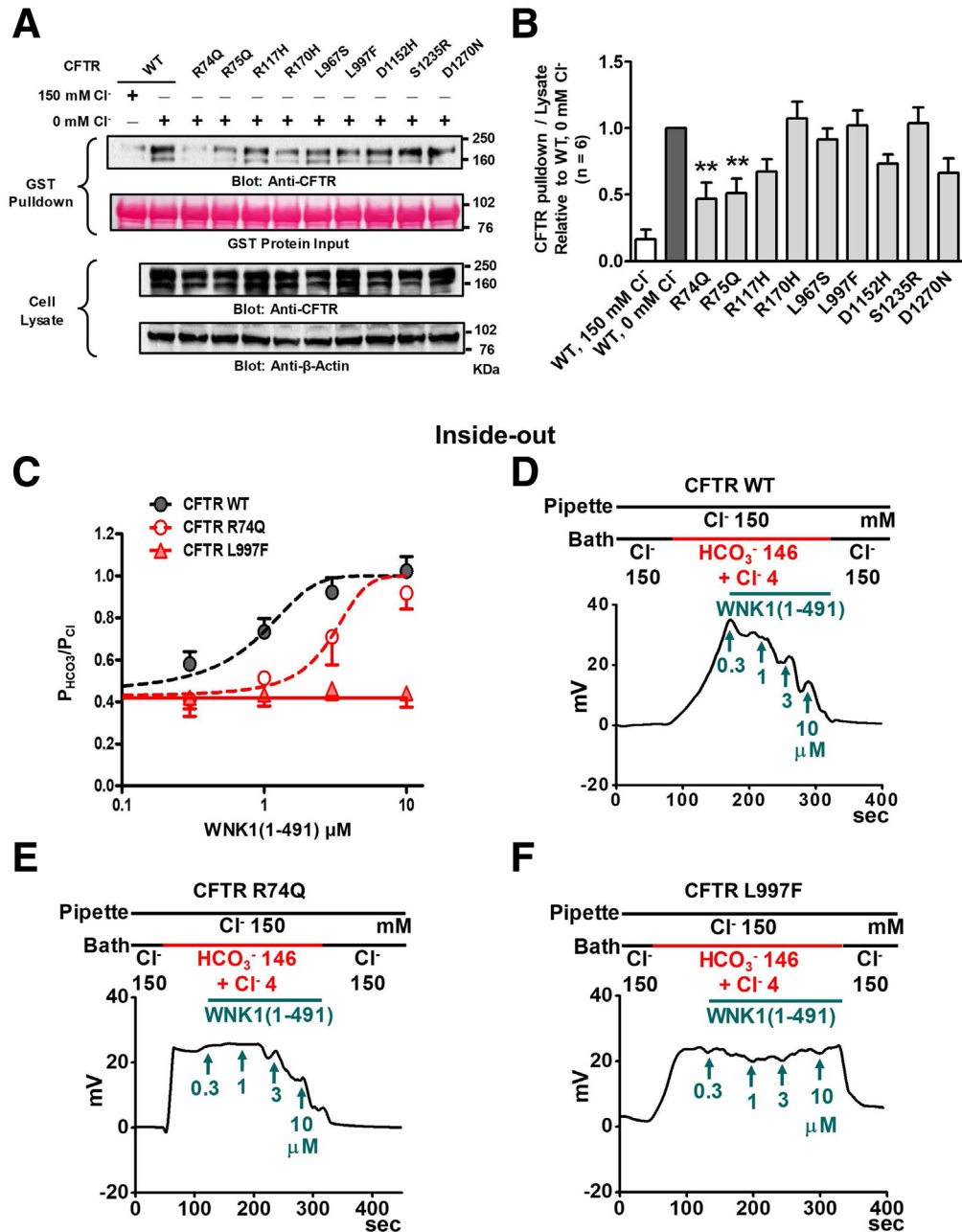


Figure 16. Molecular pathogenic mechanisms of CFTR mutations that impair WNK1-regulated HCO₃⁻ permeation. (A, B) Semi-pull-down assays were performed with recombinant GST-WNK1(1–491) and cell lysates prepared from HEK293T cells expressing CFTR. The GST pull-down assays were performed in Cl⁻-free and high-Cl⁻ (150 mM) media. The pull-down results under the 150-mM and 0-mM Cl⁻ conditions using WT CFTR-expressing cell lysates were used as negative and positive controls, respectively. Representative blots are shown in panel A, and a summary of CFTR pull-down values relative to those of WT CFTR at 0-mM Cl⁻ is illustrated in panel B (n = 6). Two CFTR mutations, R74Q and R75Q, reduced WNK1-CFTR associations. (C–F) Membrane potential was measured in inside-out patch clamp recordings using patch membranes prepared from HEK293T cells expressing WT and mutant CFTRs. Inside-out patch clamp recordings were performed using the same protocols used in Figure 12D. A summary of 5 independent experiments is shown in panel C, and representative traces are shown in panels D–F. Higher concentrations of WNK1(1–491) increased the $P_{HCO_3^-}/P_{Cl^-}$ of the CFTR R74Q mutant, but not that of the CFTR L997F mutant. Bar-graph data are presented as the mean \pm SEM. ***P* < .01: difference from CFTR alone.

G_{CFTR} in HCO₃⁻-rich solutions (Figure 4) is not anticipated to influence the membrane potential measurements. These technical maneuvers and results suggest that our data were not greatly affected by problems resulting from bi-ionic potential measurements.

The CFTR-expressing epithelial cells in the gastrointestinal, respiratory, and genitourinary systems secrete HCO₃⁻-containing fluids.^{2,7} A number of studies have shown that HCO₃⁻ in secreted fluids has diverse physiological roles, such as the prevention of mucin aggregation and mucus

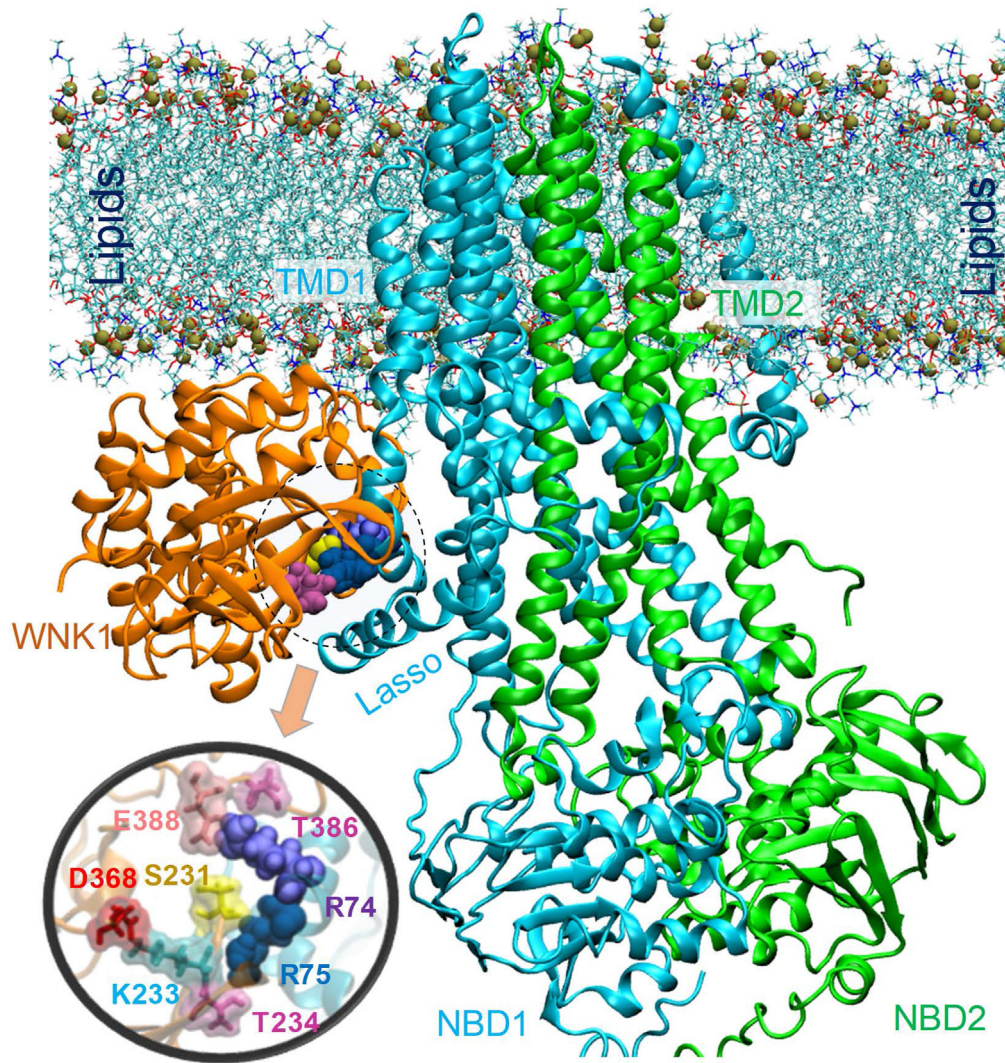


Figure 17. Structural model for the MD-equilibrated complex between hCFTR and WNK1 kinase domain in the presence of lipid bilayer. The R74 (purple balls) and R75 (blue balls) residues from hCFTR participate in the binding interface. The figure displays the hCFTR-WNK1 complex predicted by ClusPro, after equilibration in the MD simulation system where it is embedded into the membrane lipids (lines with their phosphorus atoms shown in tan spheres) and solvated by 0.1 M NaCl solution. The snapshot was taken after 100-ns MD simulations. The inset figure shows a closeup view of interfacial interactions. WNK1 residues at the interface include S231, F232, K233, T234, and I384, G385, T386 and E388.

plug formation to maintain ductal-tree patency in epithelial organs, the generation of an optimal pH environment for the enzymes and structural proteins dissolved in secreted fluids, and the prevention of overt infection and inflammation via the antibacterial properties of HCO_3^- .^{2,40,41} Consequently, aberrant HCO_3^- secretion caused by generalized defects in CFTR function, such as defective cell-surface expression and channel gating, is associated with a wide spectrum of diseases including cystic fibrosis, bronchiectasis, congenital bilateral absence of the vas deferens, and pancreatitis.^{2,42,43} Many epithelial cells, including those in sweat glands and airways, retain $>20\text{-mM}$ $[\text{Cl}^-]_i$ mostly due to the basolateral NKCC activity.^{11,44,45} On the contrary, human and guinea pig pancreatic duct cells have very low or no NKCC activity, and their $[\text{Cl}^-]_i$ can be decreased to $\sim 5\text{ mM}$ during cAMP stimulations,^{2,14,22} suggesting that a low

$[\text{Cl}^-]_i$ -induced WNK1 activation may substantially function in these cells.

Of particular interest is a recent study showing that CFTR mutants with selective defects in WNK1-regulated HCO_3^- permeation increase the risks of pancreatitis, rhinosinusitis, and male infertility.⁶ Interestingly, the R74Q and L997F mutations exhibit almost normal CFTR Cl^- channel activity,⁶ implying that CFTR functions other than Cl^- channel activity may be critical for the pathogenesis. The disease-causing R74, R75, and L997 CFTR loci are evolutionarily conserved and if mutated, impaired function would be expected. In fact, a previous study examining the clinical phenotypes of complex heterozygous individuals with L997F mutation found that L997 is highly conserved among species and suggested that the L997F mutation may exert a greater influence on CFTR

functions other than Cl⁻ transport.⁴⁶ Our molecular and electrophysiological results support the idea that R74Q reduces CFTR HCO₃⁻ channel activity by inhibiting physical associations between WNK1 and CFTR, whereas L997F does so by causing other intrinsic defects in the channel. The discoveries described in the present study will help investigators to develop better drugs and help physicians to treat patients with diseases caused by aberrant CFTR-mediated HCO₃⁻ transport, such as chronic pancreatitis.

Materials and Methods

Plasmids, Small Interfering RNAs, and Cell Culture

The mammalian-expressible plasmids for rWNK1, mSPAK, hOSR1, and hCFTR were previously described.^{14,16} HEK293T cells were cultured in Dulbecco's modified Eagle medium-high glucose (Invitrogen, Carlsbad, CA) supplemented with 10% (v/v) fetal bovine serum, 100-U/mL penicillin, and 0.1-mg/mL streptomycin. The WNK1 fragments were subcloned into a pCMV-myc plasmid or pGEX-4T1 plasmid using polymerase chain reaction amplification. The WNK1 mutant and CFTR mutant plasmids were generated using polymerase chain reaction-based site-directed mutagenesis. The small interfering RNAs against OSR1 and SPAK were purchased from GE Dharmacon (Lafayette, CO). Plasmids were transiently transfected into cells using Lipofectamine Plus (Invitrogen). siRNAs were transiently transfected into HEK293T cells using Lipofectamine 2000 (Invitrogen). An average transfection rate over 90% was confirmed by cotransfection with a plasmid expressing green fluorescent protein (GFP).

Antibodies and Immunoblot Analysis

The antibodies against SPAK (#2281; Cell Signalling Technology, Danvers, MA), OSR1 (#3729; Cell Signalling Technology), CFTR (M3A7; Upstate Biotechnology, Waltham, MA), Flag epitope (F3165; Sigma-Aldrich, St. Louis, MO), Myc epitope (sc-40; Santa Cruz Biotechnology, Santa Cruz, CA), anti-Aldolase A (ab78339; Abcam, Cambridge, United Kingdom), and β -actin (sc-1616; Santa Cruz Biotechnology) were obtained from commercial companies. For immunoblot analysis, transfected HEK293T cells were washed 3 times with ice-cold phosphate-buffered saline and then harvested with lysis buffer consisting of 50-mM Tris-HCl (pH 7.4), 150-mM NaCl, 10% (v/v) glycerol, 1% (v/v) Triton X-100, 5-mM EDTA, 5-mM EGTA, and complete protease inhibitor cocktail (Roche Applied Science, Mannheim, Germany). The cells were centrifuged, the cell lysates were diluted in 2 \times sodium dodecyl sulfate (SDS) sample buffer, and the protein samples were separated by SDS-polyacrylamide gel electrophoresis. The separated proteins were transferred to a nitrocellulose membrane and blotted with the appropriate primary and secondary antibodies. Protein bands were detected by enhanced chemiluminescence (Amersham Biosciences, Piscataway, NJ).

GST-Tagged WNK1 Proteins and Pull-Down Assays

The glutathione S-transferase (GST) pull-down assays were performed by collecting binding partners of the GST-tagged proteins as described previously.²³ The GST-tagged recombinant proteins were expressed in *Escherichia coli* BL21 transformed with pGEX-4T1-empty or pGEX-4T1-WNK1 fragment vector and purified with glutathione-Sepharose 4B (Amersham Biosciences). For the pull-down assays, HEK293T cells transfected with WT or mutant CFTR plasmids were harvested with a lysis buffer containing 50-mM Tris-Cl (pH 7.4; containing 41.2-mM free Cl⁻), 109.8-mM NaCl, 10% (v/v) glycerol, 1% (v/v) Triton X-100, 5-mM EDTA, 5-mM EGTA, and a complete protease inhibitor cocktail (Roche Applied Science). The 0-, 4-, 10-, 20-, and 40-mM Cl⁻-containing lysis buffers were prepared by replacing Cl⁻ with an equimolar concentration of gluconate using Na⁺-gluconate and Tris-gluconate. The harvested lysate supernatants were mixed with GST-WNK1 fragments bound to glutathione-Sepharose beads and incubated overnight at 4°C. The bead complexes were washed 3 times, eluted in a 2 \times sample buffer, and immunoblotted as described.

For the patch clamp experiments, recombinant GST-WNK1 fragment proteins were eluted with GST-elution buffer consisting of 50-mM Tris-HCl, 150-mM NaCl, 50-mM GSH, 1-mM DTT, and complete protease inhibitor cocktail (Roche Applied Science) (pH 8.0). The eluted GST-WNK1 fragment proteins were dialyzed with Slide-A-Lyzer dialysis cassettes (Thermo Fisher Scientific, Waltham, MA).

Surface Biotinylation Assay

After transfection with the indicated plasmids, HEK293T cells were washed 3 times with phosphate-buffered saline. The plasma membrane proteins were biotinylated by gently shaking the cells in a borate buffer containing sulfo-NHS-SS-biotin (Thermo Fisher Scientific, 21331) for 30 minutes. After the biotinylation reaction was complete, the cells were washed extensively with quenching buffer (1% bovine serum albumin solution) to remove excess biotin, followed by 2 phosphate-buffered saline washes. The cells were lysed with lysis buffer (50-mM Tris-HCl, pH 7.4, 150-mM NaCl, 1% [v:v] Nonidet P-40, 0.25% [v:v] sodium deoxycholate, and a complete protease inhibitor mixture) followed by overnight incubation at 4°C with an avidin solution (UltraLink Immobilized NeutrAvidin Beads 10%; Fisher Scientific; 53150). Avidin-bound complexes were pelleted (15,700 *g*, 20 minutes) and washed 3 times with lysis buffer. The biotinylated protein was then eluted at 37°C in a 2 \times SDS sample buffer for 40 minutes. The eluted protein was separated by SDS-polyacrylamide gel electrophoresis, electrotransferred, and immunoblotted with the indicated antibodies.

Electrophysiology

Whole-Cell Recordings. Whole-cell recordings were performed on CFTR transfected HEK293T cells as previously described.⁴⁷ Cells were transferred to a bath mounted on the stage of an inverted microscope (IX71; Olympus, Tokyo,

Japan). We selected cells showing coexpressed GFP for electrophysiological recordings. Capillary glass pipettes were prepared using a conventional micropipette puller (P-97; Sutter Instrument, Novato, CA). Patch pipettes were polished with a microforge to a resistance of $\sim 2\text{--}4\text{ M}\Omega$ in bath solutions that were connected to the head stage of a patch clamp amplifier (Axopatch-200B; Molecular Devices, Sunnyvale, CA, USA). The whole-cell patch was achieved by rupturing the membrane after giga ohm sealing. The bath solution was perfused at 5 mL/min and the voltage and current recordings were performed at room temperature ($21\text{--}23^\circ\text{C}$). In these experiments, a reference electrode was placed in a chamber containing a 3 M KCl solution, which was connected to the bath via a 1.5% (wt/vol) salt agar bridge. The bath solution contained (in mM) 146 N-methyl-D-glucamine chloride (NMDG-Cl), 1 CaCl₂, 1 MgCl₂, 5 glucose, and 10 HEPES adjusted to pH 7.4 with NMDG. The high HCO₃⁻-containing bath solution was prepared by replacing NMDG-Cl with an equimolar concentration of choline bicarbonate. The high HCO₃⁻-containing solution was continuously gassed with 95% O₂ and 5% CO₂ (pH 8.2), which is comparable to the ionic composition of human pancreatic juice.¹⁴ It has been shown that changes in pH and CO₂ concentrations do not significantly affect CFTR $P_{\text{HCO}_3^-}/P_{\text{Cl}^-}$ values.¹⁶ The low Cl⁻-containing pipette solutions were prepared by replacing Cl⁻ with an equimolar concentration of gluconate. The standard gluconate solution (10-mM Cl⁻) contained (in mM) 140 NMDG-gluconate, 8 NMDG-Cl, 5 EGTA, 1 MgCl₂, 3 MgATP, and 10 HEPES (pH 7.4). CFTR currents were activated by cAMP (5- μM forskolin and 100- μM 3-isobutyl-1-methylxanthine [IBMX]). pClamp 10.2 and Digidata 1550B (Molecular Devices) were used to acquire data and apply command pulses. The currents were filtered at 2 kHz and sampled at 500 Hz. $P_{\text{HCO}_3^-}/P_{\text{Cl}^-}$ was determined from the zero-current clamped reversal potential shift [$\Delta E_{\text{rev}} = E_{\text{rev}}(\text{HCO}_3^-) - E_{\text{rev}}(\text{Cl}^-)$], induced by replacing the extracellular Cl⁻ with HCO₃⁻ and using the Goldman-Hodgkin-Katz equation. During the zero-current clamp recording, we occasionally applied a ramp pulse (-80 to $+80$ mV, 0.8-mV/ms holding potential, near the resting membrane potential) to obtain the I-V relationship to confirm the characteristics of the measured currents. For the anion permeability test, individual data were corrected by measuring the offset potential shift induced by the replacement of the anion solution after each experiment.^{6,14,16}

Macroscopic Excised Patch Experiments. For recording of macroscopic currents in excised patch clamp experiments, pipettes with a free-tip resistance of $\sim 2\text{--}5\text{ M}\Omega$ were used. In outside-out patch recordings, the low Cl⁻-containing pipette solutions were prepared by replacing Cl⁻ with an equimolar concentration of gluconate as described previously. The ATP (3 mM)-containing pipette solutions also contained the catalytic subunit of protein kinase A (PKA) (10 U/mL; Promega, Madison, WI, USA) to activate CFTR currents. The bath solution contained (in mM) 146 NMDG-Cl, 1 CaCl₂, 1 MgCl₂, 5 glucose, and 10 HEPES (pH 7.4). The high HCO₃⁻-containing bath solution was

prepared by replacing NMDG-Cl with an equimolar concentration of choline bicarbonate. For outside-out patch recording, we first selected cells showing PKA-activated CFTR currents at whole-cell configurations. Afterward, these patches were made to outside-out patches by moving the pipette away from the cell. To determine the I-V relationship during zero-current recordings, the clamp mode was shifted to voltage clamp mode, and the I-V relationship was obtained by applying a ramp pulse from -80 to $+80$ mV (0.8 mV/ms holding potential, near the resting membrane potential). In inside-out patch clamp recordings, the pipette solution (extracellular side) contained (in mM) 146 NMDG-Cl, 1 MgCl₂, 1 CaCl₂, 10 Glucose, and 10 HEPES (pH 7.4). The initial high Cl⁻-containing bath solution (intracellular side) contained (in mM) 148 NMDG-Cl, 1 MgCl₂, 3 MgATP, 5 EGTA, and 10 HEPES, and were adjusted to pH 7.4 using NMDG. The high HCO₃⁻-containing bath solution was prepared by replacing NMDG-Cl with an equimolar concentration of choline bicarbonate. The CFTR channel was activated by the addition of the catalytic subunit of PKA (10 U/mL) to the ATP (3 mM)-containing bath solution. For anion permeability measurements in Figure 12, 150 Cl⁻ in the bath solution was replaced with $146\text{X}^- + 4\text{Cl}^-$, where X⁻ is the substitute anion (I⁻, NO₃⁻, or HCO₃⁻ in the form of NaX). The Na⁺ permeability was low and did not significantly alter under all experimental conditions ($P_{\text{Na}^+}/P_{\text{Cl}^-} \sim 0.08$), and thus the $P_{\text{X}^-}/P_{\text{Cl}^-}$ values were not corrected for the Na⁺ permeability. The macroscopic CFTR currents were filtered at 2 kHz and sampled at 500 Hz.

Single-Channel Recording. Glass coverslips containing cells co-transfected with hCFTR and GFP were placed in a chamber. Single-channel current recordings were done in excised, inside-out patches in HEK293T cells, as reported earlier.⁴⁷ Electrode resistance was kept at 15–20 M Ω for single-channel recordings. The holding potential used in the single-channel CFTR recordings was -60 mV; in some experiments, the membrane potential was held from -100 to $+100$ mV for the estimation of the I-V relationship. The pipette solution (extracellular side) contained (in mM) 146 NMDG-Cl, 1 MgCl₂, 1 CaCl₂, 10 Glucose, and 10 HEPES (pH 7.4). The initial high Cl⁻-containing bath solution (intracellular side) contained (in mM) 148 NMDG-Cl, 1 MgCl₂, 3 MgATP, 5 EGTA, and 10 HEPES (pH 7.4). The high HCO₃⁻-containing bath solution was prepared by replacing NMDG-Cl with an equimolar concentration of choline bicarbonate. The CFTR channel was activated by the addition of the catalytic subunit of PKA (10–40 U/mL, Promega), adjusting the initial P_o to approximately $\sim 0.2\text{--}0.3$. Current traces were low-pass filtered at 1 kHz during the recording and were sampled at 500 Hz. Command potential and data acquisition were controlled by pClamp 10.2 software (Axon Instruments). After reaching the steady state of CFTR single-channel currents, the data of all experiments were obtained and analyzed. The traces were further filtered with a 100-Hz cutoff frequency for data analysis and presentation. Reversal potential (E_{rev}) and slope conductance data were determined from linear I-V plots by linear regression analysis. Bicarbonate

permeability ratios were calculated from E_{rev} values using the Goldman-Hodgkin-Katz equation.

All experiments were performed at room temperature (20–23°C).

Computational Prediction of hCFTR-WNK1 Complexes

Homology Modeling of Phosphorylated, ATP-Bound Structure of Human CFTR. Pairwise sequence alignment of human CFTR (hCFTR) and zebrafish CFTR was performed using Clustal Omega (<https://www.ebi.ac.uk/Tools/msa/clustalo/>). Homology models for hCFTR in the phosphorylated, ATP-bound state were generated using MODELLER⁴⁸ based on the resolved structure of zebrafish homolog (PDB: 5W81).³⁵ A set of 100 homology models of hCFTR (composed of the segments M1–G404, T438–S642, W846–P888, T910–G1173, and D1202–K1457) were constructed; and the conformer with the best score (based on MODELLER objective function) was selected for subsequent protein-protein docking analyses.

Modeling of hCFTR-WNK1 Complex Structure. We modeled *in silico* the hCFTR-WNK1 protein complex using ClusPro.⁴⁹ The cryo-EM structure of dephosphorylated hCFTR (PDB ID: 5UAK) as well as the homology-modeled phosphorylated conformer were used as receptors; for the ligand, we employed WNK1 monomers deposited in the PDB (PDB ID: 5DRB).³⁶ Only the resolved protein structures from hCFTR and WNK1 were used, and the bound chlorides or inhibitors were not included in the docking analysis. For each simulation performed with a different WNK1 monomer, up to 30 hCFTR-WNK1 models were predicted by ClusPro. These were rank-ordered based on the docking score from ClusPro, together with 3 criteria specific to the hCFTR-WNK1 complex in a lipid environment: (1) WNK1 should bind from the intracellular region [ie, extracellular-bound forms were excluded]; (2) the hCFTR-WNK1 complex should have proper orientation of the aromatic residues (ie, Trp) on the extracellular and intracellular sides to enable suitable anchoring into the lipids; and (3) the β -sheet portion of WNK1 should not be buried in the membrane. Figure 17 displays the best conformer that meets those criteria, stabilized by molecular dynamics (MD) simulations (see below). The hCFTR regions near R74–R75 showed a strong affinity to bind WNK1. Notably, both phosphorylated and dephosphorylated hCFTR conformers showed similar binding pose onto WNK1 near R74–R75. We selected the phosphorylated hCFTR-WNK1 complex for further refinement with MD simulations.

Refinement of the hCFTR-WNK1 Complex Structure in the Lipid Environment With MD Simulations. The simulation systems were prepared using CHARMM-GUI Membrane Builder.⁵⁰ The transmembrane portion of the hCFTR-WNK1 complex was inserted into the center of a DDPC lipid bilayer, avoiding the insertion of WNK1 into the lipids. Fully equilibrated TIP3 waters were added to form a rectangular box of 133 × 133 × 182 Å³. The simulation system consisted of hCFTR, the WNK1 kinase domain, 500

DDPC molecules, and about 74,000 water molecules summing up to a total of ~293,000 atoms. Simulations were performed using NAMD (version 2.9)⁵¹ and CHARMM36 force field with CMAP corrections.^{52,53} The simulation protocol followed our previous approach.⁵⁴ The initial MD system was first energy-minimized for 50,000 steps, followed by 0.5 ns constant volume and temperature (T = 310K) simulations and a subsequent 4-ns Nosé-constant pressure and temperature (1 bar, 310 K) simulation, during which the protein was fixed and constraints on the DDPC head groups were gradually released. Subsequently, the constraints on the protein backbone were reduced from 10 kcal/mol to none within 3 ns. Finally, the unconstrained protein was subjected to NPT simulations for 100 ns. Two independent runs were performed. In both cases, the root-mean-square deviation of C α atoms from the original structure converged to 5.0 ± 0.3 Å after 50 ns, indicating the formation of stable complex in the presence of the lipid bilayer. Figure 17 illustrates the simulation system equilibrated after a 100 ns run.

Statistical Analysis

The results of multiple experiments are presented as the mean ± SEM. Statistical analysis was performed with Student's *t* test or by analysis of variance followed by Tukey's multiple comparison test, as appropriate. We considered *P* < .05 to be statistically significant.

References

1. Case RM, Harper AA, Scratcherd T. The secretion of electrolytes and enzymes by the pancreas of the anaesthetized cat. *J Physiol* 1969;201:335–348.
2. Lee MG, Ohana E, Park HW, Yang D, Muallem S. Molecular mechanism of pancreatic and salivary gland fluid and HCO₃⁻ secretion. *Physiol Rev* 2012;92:39–74.
3. Reddy MM, Quinton PM. Control of dynamic CFTR selectivity by glutamate and ATP in epithelial cells. *Nature* 2003;423:756–760.
4. Lee MG, Muallem S. Physiology of duct cell secretion. In: Beger H, Buchler M, Kozarek R, Lerch M, Neoptolemos J, Warshaw A, Whitcomb D, Shiratori K, Rau BM, eds. *Pancreas: An Integrated Textbook of Basic Science, Medicine, and Surgery*. Oxford, United Kingdom: Blackwell, 2008:78–90.
5. Chen EY, Yang N, Quinton PM, Chin WC. A new role for bicarbonate in mucus formation. *Am J Physiol Lung Cell Mol Physiol* 2010;299:L542–L549.
6. LaRusch J, Jung J, General IJ, Lewis MD, Park HW, Brand RE, Gelrud A, Anderson MA, Banks PA, Conwell D, Lawrence C, Romagnuolo J, Baillie J, Alkaade S, Cote G, Gardner TB, Amann ST, Slivka A, Sandhu B, Aloe A, Kienholz ML, Yadav D, Barnada MM, Bahar I, Lee MG, Whitcomb DC, North American Pancreatitis Study G. Mechanisms of CFTR functional variants that impair regulated bicarbonate permeation and increase risk for pancreatitis but not for cystic fibrosis. *PLoS Genet* 2014;10:e1004376.

7. Steward MC, Ishiguro H, Case RM. Mechanisms of bicarbonate secretion in the pancreatic duct. *Annu Rev Physiol* 2005;67:377–409.
8. Park S, Shcheynikov N, Hong JH, Zheng C, Suh SH, Kawaai K, Ando H, Mizutani A, Abe T, Kiyonari H, Seki G, Yule D, Mikoshiba K, Muallem S. Irbit mediates synergy between Ca^{2+} and cAMP signaling pathways during epithelial transport in mice. *Gastroenterology* 2013;145:232–241.
9. Yang D, Shcheynikov N, Zeng W, Ohana E, So I, Ando H, Mizutani A, Mikoshiba K, Muallem S. IRBIT coordinates epithelial fluid and HCO_3^- secretion by stimulating the transporters pNBC1 and CFTR in the murine pancreatic duct. *J Clin Invest* 2009;119:193–202.
10. Ko SB, Shcheynikov N, Choi JY, Luo X, Ishibashi K, Thomas PJ, Kim JY, Kim KH, Lee MG, Naruse S, Muallem S. A molecular mechanism for aberrant CFTR-dependent HCO_3^- transport in cystic fibrosis. *EMBO J* 2002;21:5662–5672.
11. Whitcomb DC, Ermentrout GB. A mathematical model of the pancreatic duct cell generating high bicarbonate concentrations in pancreatic juice. *Pancreas* 2004;29:e30–e40.
12. Park HW, Lee MG. Transepithelial bicarbonate secretion: lessons from the pancreas. *Cold Spring Harb Perspect Med* 2012;2:a009571.
13. Ishiguro H, Steward MC, Naruse S, Ko SB, Goto H, Case RM, Kondo T, Yamamoto A. CFTR functions as a bicarbonate channel in pancreatic duct cells. *J Gen Physiol* 2009;133:315–326.
14. Park HW, Nam JH, Kim JY, Namkung W, Yoon JS, Lee JS, Kim KS, Venglovecz V, Gray MA, Kim KH, Lee MG. Dynamic regulation of CFTR bicarbonate permeability by $[\text{Cl}^-]_i$ and its role in pancreatic bicarbonate secretion. *Gastroenterology* 2010;139:620–631.
15. Riordan JR, Rommens JM, Kerem B, Alon N, Rozmahel R, Grzelczak Z, Zielenski J, Lok S, Plavsic N, Chou JL, Drumm ML, Iannuzzi MC, Collins FS, Tsui L-C. Identification of the cystic fibrosis gene: cloning and characterization of complementary DNA. *Science* 1989;245:1066–1073.
16. Jun I, Cheng MH, Sim E, Jung J, Suh BL, Kim Y, Son H, Park K, Kim CH, Yoon JH, Whitcomb DC, Bahar I, Lee MG. Pore dilatation increases the bicarbonate permeability of CFTR, ANO1 and glycine receptor anion channels. *J Physiol* 2016;594:2929–2955.
17. Tang L, Fatehi M, Linsdell P. Mechanism of direct bicarbonate transport by the CFTR anion channel. *J Cyst Fibros* 2009;8:115–121.
18. Sohma Y, Gray MA, Imai Y, Argent BE. HCO_3^- transport in a mathematical model of the pancreatic ductal epithelium. *J Membr Biol* 2000;176:77–100.
19. Piala AT, Moon TM, Akella R, He H, Cobb MH, Goldsmith EJ. Chloride sensing by WNK1 involves inhibition of autophosphorylation. *Sci Signal* 2014;7:ra41.
20. Richardson C, Sakamoto K, de los Heros P, Deak M, Campbell DG, Prescott AR, Alessi DR. Regulation of the NKCC2 ion cotransporter by SPAK-OSR1-dependent and -independent pathways. *J Cell Sci* 2011;124:789–800.
21. Wakabayashi M, Mori T, Isobe K, Sohara E, Susa K, Araki Y, Chiga M, Kikuchi E, Nomura N, Mori Y, Matsuo H, Murata T, Nomura S, Asano T, Kawaguchi H, Nonoyama S, Rai T, Sasaki S, Uchida S. Impaired KLHL3-mediated ubiquitination of WNK4 causes human hypertension. *Cell Rep* 2013;3:858–868.
22. Ishiguro H, Naruse S, Kitagawa M, Mabuchi T, Kondo T, Hayakawa T, Case RM, Steward MC. Chloride transport in microperfused interlobular ducts isolated from guinea-pig pancreas. *J Physiol* 2002;539:175–189.
23. Jung J, Nam JH, Park HW, Oh U, Yoon JH, Lee MG. Dynamic modulation of ANO1/TMEM16A HCO_3^- permeability by Ca^{2+} /calmodulin. *Proc Natl Acad Sci U S A* 2013;110:360–365.
24. Schneider A, Larusch J, Sun X, Aloe A, Lamb J, Hawes R, Cotton P, Brand RE, Anderson MA, Money ME, Banks PA, Lewis MD, Baillie J, Sherman S, Disario J, Burton FR, Gardner TB, Amann ST, Gelrud A, George R, Rockacy MJ, Kassabian S, Martinson J, Slivka A, Yadav D, Oruc N, Barmada MM, Frizzell R, Whitcomb DC. Combined bicarbonate conductance-impairing variants in CFTR and SPINK1 variants are associated with chronic pancreatitis in patients without cystic fibrosis. *Gastroenterology* 2011;140:162–171.
25. Wang HR, Liu Z, Huang CL. Domains of WNK1 kinase in the regulation of ROMK1. *Am J Physiol Renal Physiol* 2008;295:F438–F445.
26. Xu B, English JM, Wilsbacher JL, Stippec S, Goldsmith EJ, Cobb MH. WNK1, a novel mammalian serine/threonine protein kinase lacking the catalytic lysine in subdomain II. *J Biol Chem* 2000;275:16795–16801.
27. Terker AS, Zhang C, Erspamer KJ, Gamba G, Yang CL, Ellison DH. Unique chloride-sensing properties of WNK4 permit the distal nephron to modulate potassium homeostasis. *Kidney Int* 2016;89:127–134.
28. Shcheynikov N, Son A, Hong JH, Yamazaki O, Ohana E, Kurtz I, Shin DM, Muallem S. Intracellular Cl^- as a signaling ion that potently regulates $\text{Na}^+/\text{HCO}_3^-$ transporters. *Proc Natl Acad Sci U S A* 2015;112:E329–E337.
29. Yu Y, Kuan AS, Chen TY. Calcium-calmodulin does not alter the anion permeability of the mouse TMEM16A calcium-activated chloride channel. *J Gen Physiol* 2014;144:115–124.
30. Anderson MP, Welsh MJ. Calcium and cAMP activate different chloride channels in the apical membrane of normal and cystic fibrosis epithelia. *Proc Natl Acad Sci U S A* 1991;88:6003–6007.
31. Alessi DR, Zhang J, Khanna A, Hochdorfer T, Shang Y, Kahle KT. The WNK-SPAK/OSR1 pathway: master regulator of cation-chloride cotransporters. *Sci Signal* 2014;7:re3.
32. He G, Wang HR, Huang SK, Huang CL. Intersectin links WNK kinases to endocytosis of ROMK1. *J Clin Invest* 2007;117:1078–1087.
33. Yang CL, Zhu X, Wang Z, Subramanya AR, Ellison DH. Mechanisms of WNK1 and WNK4 interaction in the regulation of thiazide-sensitive NaCl cotransport. *J Clin Invest* 2005;115:1379–1387.

34. Yang D, Li Q, So I, Huang CL, Ando H, Mizutani A, Seki G, Mikoshiba K, Thomas PJ, Muallem S. IRBIT governs epithelial secretion in mice by antagonizing the WNK/SPAK kinase pathway. *J Clin Invest* 2011; 121:956–965.
35. Liu F, Zhang Z, Csanady L, Gadsby DC, Chen J. Molecular structure of the human CFTR ion channel. *Cell* 2017;169:85–95.e8.
36. Yamada K, Park HM, Rigel DF, DiPetrillo K, Whalen EJ, Anisowicz A, Beil M, Berstler J, Brocklehurst CE, Burdick DA, Caplan SL, Capparelli MP, Chen G, Chen W, Dale B, Deng L, Fu F, Hamamatsu N, Harasaki K, Herr T, Hoffmann P, Hu QY, Huang WJ, Idamakanti N, Imase H, Iwaki Y, Jain M, Jeyaseelan J, Kato M, Kaushik VK, Kohls D, Kunjathoor V, LaSala D, Lee J, Liu J, Luo Y, Ma F, Mo R, Mowbray S, Mogi M, Ossola F, Pandey P, Patel SJ, Raghavan S, Salem B, Shanado YH, Trakshel GM, Turner G, Wakai H, Wang C, Weldon S, Wielicki JB, Xie X, Xu L, Yagi YI, Yasoshima K, Yin J, Yowe D, Zhang JH, Zheng G, Monovich L. Small-molecule WNK inhibition regulates cardiovascular and renal function. *Nat Chem Biol* 2016;12:896–898.
37. Reddy MM, Quinton PM. Selective activation of cystic fibrosis transmembrane conductance regulator Cl⁻ and HCO₃⁻ conductances. *J Pancreas* 2001;2:212–218.
38. Smith SS, Steinle ED, Meyerhoff ME, Dawson DC. Cystic fibrosis transmembrane conductance regulator. Physical basis for lyotropic anion selectivity patterns. *J Gen Physiol* 1999;114:799–818.
39. Jung J, Lee MG. Does calmodulin regulate the bicarbonate permeability of ANO1/TMEM16A or not? *J Gen Physiol* 2015;145:75–77.
40. Quinton PM. Cystic fibrosis: impaired bicarbonate secretion and mucoviscidosis. *Lancet* 2008; 372:415–417.
41. Shah VS, Meyerholz DK, Tang XX, Reznikov L, Abou Alaiwa M, Ernst SE, Karp PH, Wohlford-Lenane CL, Heilmann KP, Leidinger MR, Allen PD, Zabner J, McCray PB Jr, Ostedgaard LS, Stoltz DA, Randak CO, Welsh MJ. Airway acidification initiates host defense abnormalities in cystic fibrosis mice. *Science* 2016; 351:503–507.
42. Wang XF, Zhou CX, Shi QX, Yuan YY, Yu MK, Ajonuma LC, Ho LS, Lo PS, Tsang LL, Liu Y, Lam SY, Chan LN, Zhao WC, Chung YW, Chan HC. Involvement of CFTR in uterine bicarbonate secretion and the fertilizing capacity of sperm. *Nat Cell Biol* 2003;5:902–906.
43. Gee HY, Noh SH, Tang BL, Kim KH, Lee MG. Rescue of DF508-CFTR trafficking via a GRASP-dependent unconventional secretion pathway. *Cell* 2011;146:746–760.
44. Macias WL, McAteer JA, Tanner GA, Fritz AL, Armstrong WM. NaCl transport by Madin Darby canine kidney cyst epithelial cells. *Kidney Int* 1992;42:308–319.
45. Willumsen NJ, Davis CW, Boucher RC. Intracellular Cl⁻ activity and cellular Cl⁻ pathways in cultured human airway epithelium. *Am J Physiol* 1989;256:C1033–C1044.
46. Lucarelli M, Narzi L, Pierandrei S, Bruno SM, Stamato A, d'Avanzo M, Strom R, Quattrucci S. A new complex allele of the CFTR gene partially explains the variable phenotype of the L997F mutation. *Genet Med* 2010; 12:548–555.
47. Lee JH, Richter W, Namkung W, Kim KH, Kim E, Conti M, Lee MG. Dynamic regulation of cystic fibrosis transmembrane conductance regulator by competitive interactions of molecular adaptors. *J Biol Chem* 2007; 282:10414–10422.
48. Sali A, Blundell TL. Comparative Protein Modeling by Satisfaction of Spatial Restraints. *J Mol Biol* 1993; 234:779–815.
49. Kozakov D, Hall DR, Xia B, Porter KA, Padhorny D, Yueh C, Beglov D, Vajda S. The ClusPro web server for protein-protein docking. *Nat Protoc* 2017; 12:255–278.
50. Jo S, Lim JB, Klauda JB, Im W. CHARMM-GUI Membrane Builder for mixed bilayers and its application to yeast membranes. *Biophys J* 2009;97:50–58.
51. Phillips JC, Braun R, Wang W, Gumbart J, Tajkhorshid E, Villa E, Chipot C, Skeel RD, Kale L, Schulten K. Scalable molecular dynamics with NAMD. *J Comput Chem* 2005; 26:1781–1802.
52. Mackerell AD Jr, Feig M, Brooks CL 3rd. Extending the treatment of backbone energetics in protein force fields: limitations of gas-phase quantum mechanics in reproducing protein conformational distributions in molecular dynamics simulations. *J Comput Chem* 2004; 25:1400–1415.
53. Klauda JB, Venable RM, Freites JA, O'Connor JW, Tobias DJ, Mondragon-Ramirez C, Vorobyov I, MacKerell AD Jr, Pastor RW. Update of the CHARMM all-atom additive force field for lipids: validation on six lipid types. *J Phys Chem B* 2010;114:7830–7843.
54. Cheng MH, Torres-Salazar D, Gonzalez-Suarez AD, Amara SG, Bahar I. Substrate transport and anion permeation proceed through distinct pathways in glutamate transporters. *Elife* 2017;6:e25850.

Received December 11, 2018. Accepted September 17, 2019.

Correspondence

Address correspondence to: Min Goo Lee, Department of Pharmacology, Yonsei University College of Medicine, 50-1 Yonsei-ro, Seoul 03722, Korea. e-mail: mlee@yuhs.ac; fax: +82 2 313 1894.

Author contributions

Y.K., acquisition and analysis of data, and drafting of the manuscript; I.J., study concept and design, and acquisition and interpretation of data; D.H.S., acquisition and interpretation of data; J.G.Y., analysis of data; H.P., acquisition of data; J.J., analysis of data; H.W.P., acquisition of data; M.H.C., analysis of data; I.B., study concept and design, and analysis of data; D.C.W., study concept and design, and analysis of data; M.G.L., study concept and design, critical revision of the manuscript, and study supervision.

Conflicts of interest

The authors disclose no conflicts.

Funding

This work was funded by grants 2013R1A3A2042197 (to Min Goo Lee) and 2015R1D1A1A01057618 (to Yonjung Kim) from the National Research Foundation of Korea, the Ministry of Science, ICT & Future Planning, Republic of Korea; and grant HI15C1543 (to Min Goo Lee) of the Korea Health Technology R&D Project through the Korea Health Industry Development Institute, funded by the Ministry of Health & Welfare, Republic of Korea. The work of Mary Hongying Cheng and Ivet Bahar was supported by National Institutes of Health grants P30DA035778 and P41GM103712.